Hochschule Karlsruhe
Technik und Wirtschaft
UNIVERSITY OF APPLIED SCIENCES

Bachelor Thesis

Low-Noise Charge Amplifier for the LEGEND-200 Cooperation

Studies Electrical Engineering and Information Technology

Hochschule Karlsruhe Technik und Wirtschaft

Author: Nikola Lukezic [51238]

Supervisor: Prof Dr. Michael Bantel

Referees: Prof. Dr. Michael Bantel

Prof. Dr. Hans Sapotta

Statutory Declaration

I declare that I have authored this thesis independently, that I have not used other than the declared sources / resources, and that I have explicitly marked all material which has been quoted either literally or by content from the used sources.

Date, Signature

Abstract

The GERDA (Germanium Detector Array) experiment at the Laboratori Nazionali del Gran Sasso (LNGS) searches for the hypothetical decay of $^{76}Ge \longrightarrow^{76} Se + 2e^{-}$, the experiment uses germanium detectors that act both as a source and a detector. The GERDA collaboration will merge with MAJORANA collaboration to build a new experiment LEGEND (The Large Enriched Germanium Experiment for Neutrinoless Double Beta Decay). These detectors are readout with charge sensitive amplifiers [1].

After a brief introduction into low noise charge amplifiers, followed by potential design of a low noise charge amplifier with minimal components and its implementation. Special care has been taken in selecting the best input FET (Field Effect Transistor) for minimal noise and reducing the input capacitance. Multiple FETs were measured and characterized, at room temperature and in liquid nitrogen. A measurement setup was built with high care to grounding, low noise equipment and reducing all external noise sources. Noise sources were monitored during measurements and eliminated if present, excluding false measurements. All measurement equipment was either tested or optimized to fit the noise criteria of the measurement system.

The amplifier was tested in various configurations, both at room temperature and in liquid nitrogen. Measurements were conducted by varying the shaping time of the digital filter. This enabled that the noise could be divided into three components, series noise, parallel noise, and $\frac{1}{f}$ noise, giving a better approximation of dominant noise sources. Multiple setups were tested, which included various input FETs and additional biasing methods. Measurements with a modeled detector gave a better approximation of realistic measurement setups.

Results showed lowest noise levels of $FWHM = 500eV$, other implementations have noise levels in the same region [2], with the amplifier proposed in this thesis having advantages such as minimal construction, low power consumption and self biasing, leading to a high variation of implementations.

List of Figures

List of Tables

Contents

1 Introduction

1.1 GERDA/LEGEND

The GERDA-experiment (GERmanium Detector Array)is searching for neutrinoless double beta decay $0\nu\beta\beta$ at the Laboratori Nazionali del Gran Sasso (LNGS). The experiment uses high purity enriched ^{76}Ge crystal diodes (HPGe) as a beta decay source and particle detectors. The HPGe detectors are submerged into a 64m^3 cryostat filled with liquid argon (LAr).The LAr serves as a cooling medium and a shield against external backgrounds. The shielding is complemented by 3m of water which is instrumented with photo multipliers to detect Cherenkov light generated by muons. The HPGe detector signals are read out with custom-made charge sensitive amplifiers optimized for low radioactivity which are operated close to the detectors in LAr. In addition to these shielding precautions the LNGS facility is located underground, reducing cosmic radiation background [5].

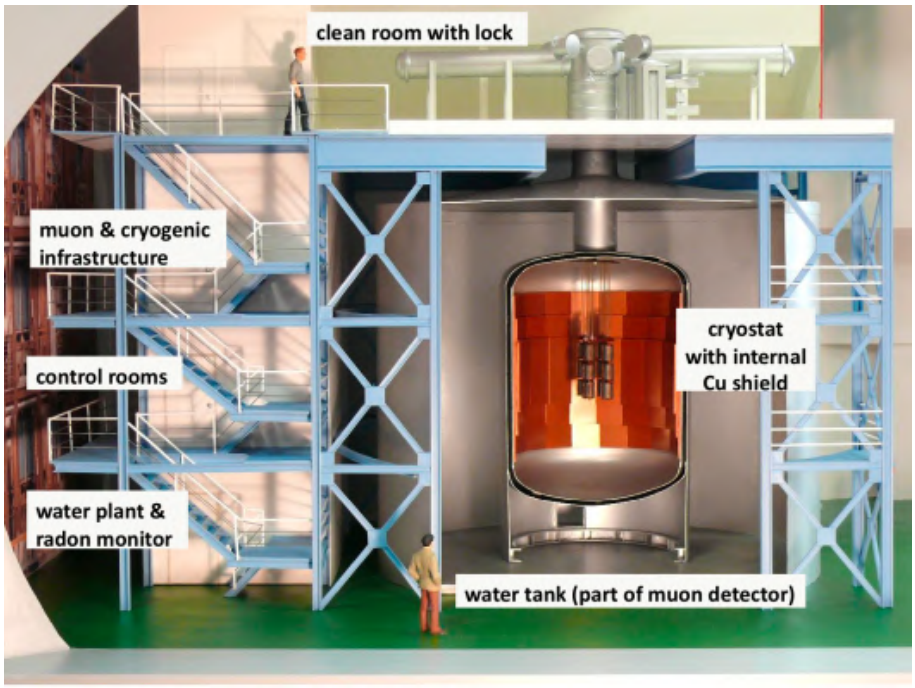

Figure 1.1: Setup of GERDA experiment [3]

The analog signals are digitized with 100 MHz Flash ADCs (Analog Digital Converter) and analyzed offline. If one of the detectors has an energy deposition above the trigger threshold (40-100 keV), all channels are analyzed for possible coincidences. After completing the GERDA experiment, the GERDA collaboration will merge with MAJORANA-collaboration to build a new experiment LEGEND (The Large Enriched Germanium Experiment for Neutrinoless Double Beta Decay)[3] .

1.2 Charge Amplifiers

Figure 1.2 shows the setup of a charge amplifier, with a detector modeled as a current source and a capacitance C_{det}. The detector delivers a short current pulse into the amplifier $i(t) = \delta(t)\ q$. The pulse is integrated into a voltage step, amplified and discharged over R_f shaping it into an exponential decay, with the time constant $\tau = R_f\ C_f$. The discharge can be realized continuously with a feedback resistor as seen in figure 1.2 or discrete with a switch that is closed shortly after every pulse[4]. Here we focus purely

on continuous discharge with a resistor. This first amplification stage is the most crucial component of the electronics chain for it defines the noise properties of the overall system, and should therefore be mounted as close as possible to the detector [6].

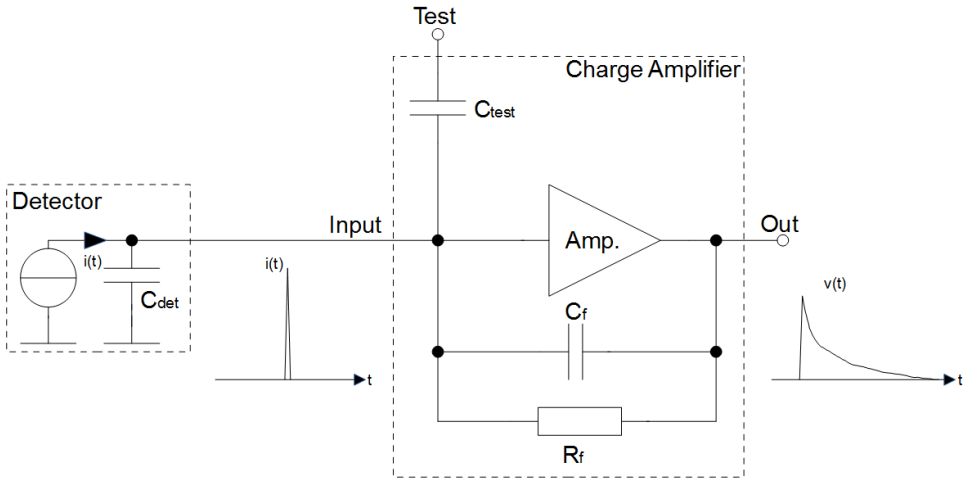

Figure 1.2: Charge amplifier setup with detector

If we consider the input of the amplifier is a FET in the common-source configuration, the input capacitance to the amplifier (Amp.) would be $C_{GS} + C_{GD}$, for best results this capacitance should not be larger than the detectors capacitance [6]. The capacitance C_{test} is used for testing and calibration of the preamplifier, therefore a step function is given to the test input, creating a current pulse, the equivalent charge can be calculated with equation 1. The amplification of a charge amplifier is shown in equation 3.

$$q = C_{test}\,\hat{V}_{test} \tag{1}$$

$$\hat{V}_{out} = \frac{q}{C_f} \tag{2}$$

$$A = \frac{\hat{V}_{out}}{\hat{V}_{test}} = \frac{C_{test}}{C_f} \tag{3}$$

The capacitance C_{test} is easily effected by stray capacitances an must be exactly determined to have the correct equivalent charge, this was done in section 4.8. Equation 3 shows the amplification of a test signal. To still achieve amplification the capacitance C_f must be kept lower then C_{test}, $C_{test} > C_f$ [4].

1.3 Electronic Noise Sources

A noise amplifier can be modelled as a noiseless amplifier with two uncorrelated noise sources, one current and one voltage source. The current source is modelled in parallel to the amplifier and is responsible for so called "parallel noise". The voltage source is modelled in series to the amplifier and is responsible for so called "series noise". Figure 1.3 shows the noiseless amplifier with its modelled noise sources, where the capacitance C_i is the total input capacitance of the preamplifier and in described by equation 4.

$$C_i = C_{GS} + C_{GD} + C_f + C_{test} + C_{wiring} \tag{4}$$

$$C_t = C_{det} + C_i \tag{5}$$

The capacitance C_{GS} is the Gate-Source capacitance of the input FET usually is the most dominant capacitance in C_i.

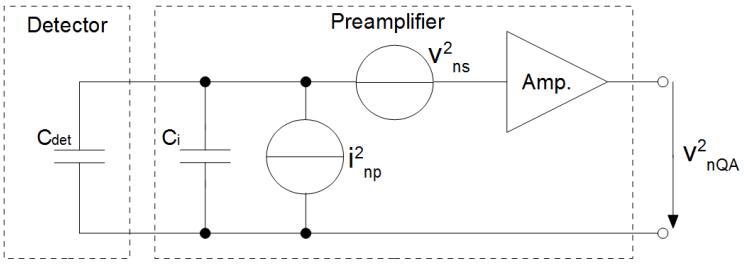

Figure 1.3: Noise model of preamplifier with detector

The sources of noise are detailed in table 1.1, the dominant and unavoidable ones are the ones from the input J-FET and the detector. The noise sources are split into "white" noise, frequency independent and colored noise, frequency dependent. Most white noise sources will be reduced by cooling, especially the detector dark current and gate current. Furthermore the dielectrics noise of the J-FET is negligible compared to other parallel noise sources, for more information see [4].

Source	Parallel Noise $[\frac{A^2}{Hz}]$	Series Noise $[\frac{V^2}{Hz}]$
	"white"	"white"
Detector	$qM^2I_{db}(1+v_M)$	
Bias resistor	$\frac{2KT}{R_b}$	
Feedback resistor	$\frac{2kT}{R_f}$	
J-FET:		
-gate current	qI_G	
-channel thermal noise		$\frac{2KT}{g_m}\frac{2}{3}$
-induced gate noise		$\frac{2KT}{g_m}\frac{1}{4}(\frac{C_{GS}}{C_t})^2$
Sub-total	b	a
	"violet"	"pink"
J-FET		$\frac{c}{\lvert\omega\rvert}$
Dielectrics	$d\lvert\omega\rvert$	
Total	$i_{np}^2 = b + d\lvert\omega\rvert \approx b$	$v_{ns}^2 = a + \frac{c}{\lvert\omega\rvert}$

Table 1.1: Noise sources in charge amplifiers [4]

$k = 1.380\ 10^{-23}\frac{J}{K}$ is the Boltzmann constant, T is the absolute temperature in kelvin, I_{db} is the dark current of the detector, variables M and v_M are detector dependent and c is device dependent.
If the series noise density v_{ns}^2 is converted to a current noise density in parallel with i_{np}^2, the total noise at the input of the preamplifier is shown in equation 6.

$$S(\omega) = a\omega^2 C_t^2 + b + c|\omega| C_t^2 \tag{6}$$

The noise at the output of the preamplifier can the be calculated with equation 7, where $G(j\omega)$ is the impulse response of the preamplifier.

$$v_{nQA}^2 = S(\omega)|G(j\omega)|^2 \tag{7}$$

If this signal is filtered with a filter with variable shaping time τ the output electronic noise Charge Q_n^2 has a course given by equation 8, for detailed calculation see [4].

$$Q_n^2 = \frac{Q_{ns}^2}{\tau} + Q_{nf}^2 + Q_{np}^2 \tau \tag{8}$$

Three noise components are present in this equation Q_{ns}^2 series noise that decreases with the increase of shaping time τ, $\frac{1}{f}$ noise Q_{nf}^2 that is not affected by the shaping time τ and Q_{np}^2 parallel noise that increases with the shaping time τ.

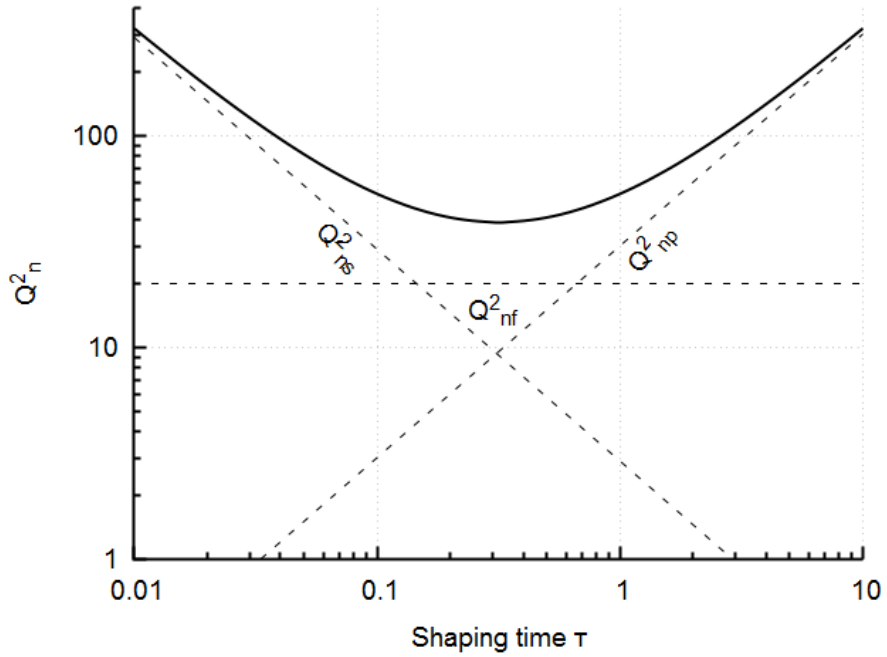

Figure 1.4: The Electronic Noise Charge Q_n^2 versus the shaping time τ

2 Circuit Design

All capitalized variables representing signals referring to dc signals and big signal calculations (V_{GS}, I_{D0}), all non capitalized signal variables refer to ac signals and small signal calculations (v_{ds}, i_{R1}).

The circuit was designed by Prof. Dr. Michael Bantel.

The charge amplifier circuit is divided into two stages one being the preamplifier, that is responsible for a small amplification and pulse shaping, this stage would be assembled directly at the detector, and the other being the post amplifier for additional amplification and biasing which can be assembled up to 10m away from the preamplifier depending on the configuration.

2.1 Preamplifier Design

The basic preamplifier consist of 6-7 JFETs, 1 MOSFET and 2 resistors. The first input stage of the preamplifier is a common-source amplifier, this leads to a very high input impedance and high gain. Figure 2.1 shows a JFET in common-source setup. The transconductance gm of a FET is given by equation 9, and is dependent on the characteristics of the FET [7], following Ohms law the gain is shown in equation 10, the common-source amplifier is an inverting amplifier, represented by the negative gain. The resistor r_0 is used for modeling the Channel length modulation, and it is present between the drain and source, and can be calculated with equation 11, the parameter λ is a device constant, typical values range from $1m\frac{1}{V}$ to $100m\frac{1}{V}$.

$$g_m = \frac{i_{out}}{v_{in}} = 2\sqrt{\frac{I_{DSS}}{V_{th}^2} I_{D0}} \tag{9}$$

$$A_S = -g_m \;\; R_D||R_L||r_0 = \frac{v_{out}}{v_{in}} \tag{10}$$

$$r_0 = \frac{1}{\lambda I_{D0}} \tag{11}$$

The second stage of the preamplifier is a common-gate amplifier, as seen in figure 2.2. Unlike the common-source amplifier the common-gate amplifier does not have a high input impedance, but has a different characteristic that is important to a preamplifier, it eliminates the miller effect and therefore lowers the total input capacitance of the preamplifier [7]. Figure 2.2 shows that $v_{gs} = -v_{in}$, therefore the voltage amplification of a common-gate amplifier is the same as a common-source amplifier, just non inverting.

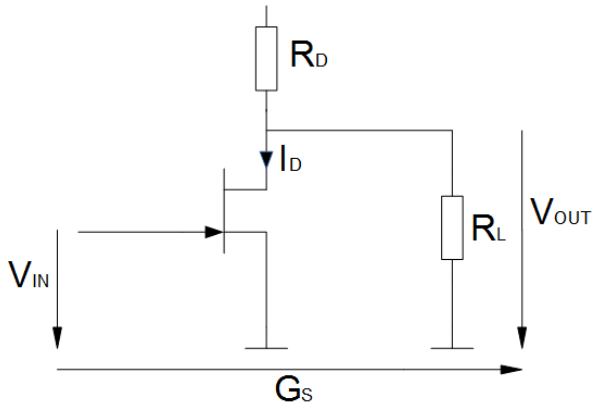

Figure 2.1: JFET in common-source amplifier layout

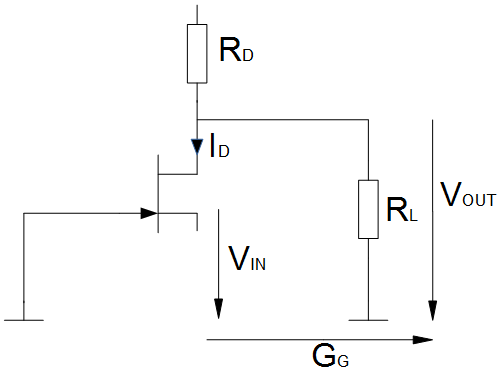

Figure 2.2: JFET in common-gate amplifier layout

These two circuits suffer from significant uncertainty of operating current, to ensure predictable biasing one can implement a current source, as the one shown in figure 2.3. Compared to a common current source, implemented without Q_2 a cascade current source seen in figure 2.3 is less affected by the load, for V_{DS} of Q_1 is biased by V_{GS} of Q_2 or $V_{DS1} = -V_{GS2}$[8]. Figure 2.4 shows a graph to help select the correct resistor for a wanted current, the gradient of the line is $-\frac{1}{R_1}$, the resulting current can be read from the interception. [7]

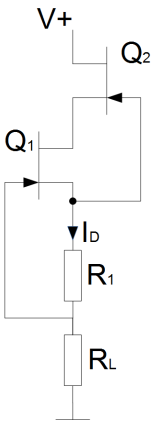

Figure 2.3: Cascade JFET current source

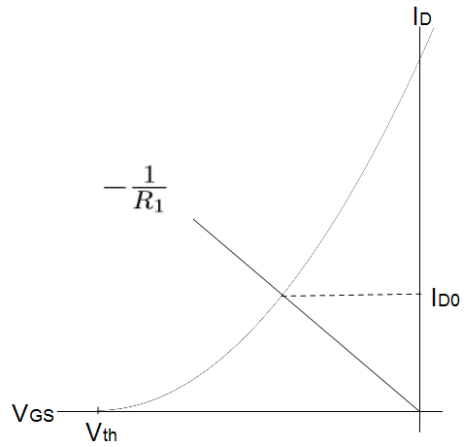

Figure 2.4: Graph for estimating R_1 for wanted I_D

Combining these three circuits in a cascade results in an amplifying stage with very high open loop gain, high input impedance, low input capacitance and high bandwidth. The simplified cascade amplifier can be seen in figure 2.5, here the current source is replaced with an ideal current source ($R = \infty$) which is a good enough assumption for this circuit. To calculate the open-loop gain the small signal model for FETs is needed, drain to source is modeled as a current source controlled by v_{gs} with a parallel resistor r_0 to model the channel length modulation. The small signal model for the cascade amplifier can be seen in figure 2.6, the open loop gain can simply be calculated by Kirchhoff's current law (KCL).

Node A

$$-g_{m2}v_{gs2} + \frac{v_{out} + v_{gs2}}{r_{02}} = 0 \tag{12}$$

$$v_{out} = g_{m2}v_{gs2}r_{02} - v_{gs2} = v_{gs2}(g_{m2}r_{02} - 1) \tag{13}$$

Node B

$$-g_{m1}v_{in} + \frac{v_{gs2}}{r_{01}} = 0 \tag{14}$$

$$v_{in} = \frac{v_{gs2}}{r_{01}g_{m1}} \tag{15}$$

This calculation is not completely correct for we assumed that the impedance of the current-source is $R = \infty$ and that $i_{out} = 0$, but it is a good enough approximation. Combining equation 13 and 15 gives the open loop gain, shown in equation 16.

$$A_0 = \frac{v_{out}}{v_{in}} = r_{01}g_{m1}(g_{m2}r_{02} - 1) \approx r_{01}r_{02}g_{m1}g_{m2} \tag{16}$$

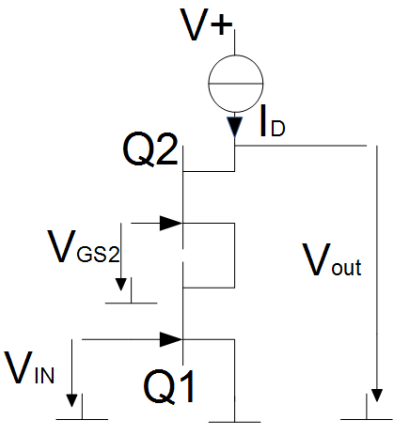

Figure 2.5: Cascode amplifier

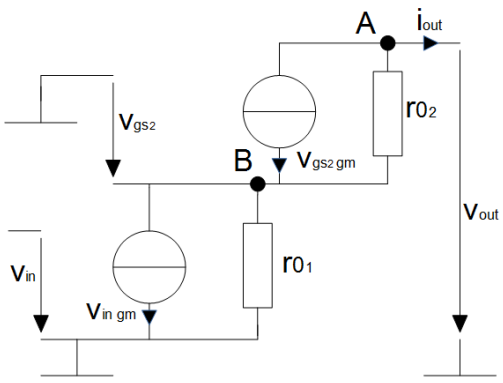

Figure 2.6: Small signal model of the cascode amplifier

Considering $Q1$ is a BF862, $Q2$ is a MMBF4416 and $I_D = 2.5mA$ as used in some of the following measurements, then the open-loop gain would be ≈ 35000. To satisfy the assumption $i_{out} \approx 0A$ a source follower is connected to the output. A source follower as the name considers follows the input, without any amplification, but has a very high input impedance that leads to $i_{out} \approx 0A$. Following the source follower is a push pull driver, as the one seen in figure 2.7 to drive up to 10m of cable. Important when designing a push-pull driver in this configuration is that the two FETs running the driver compliment each other, $V_{th1} \approx V_{th2}$, this must be true at room temperature and when operating in cryogenic state.

Figure 2.7 shows the preamplifier divided into its components. The resistor R_5 was added to bias the source follower. The capacitance C_{test}, C_f and R_f were discussed in section 1.2 and are used for calibration, testing and pulse shaping. The voltage V_{bias} is needed to keep the the FETs in the saturation region where they operate as amplifiers, and is set by the post amplifier.

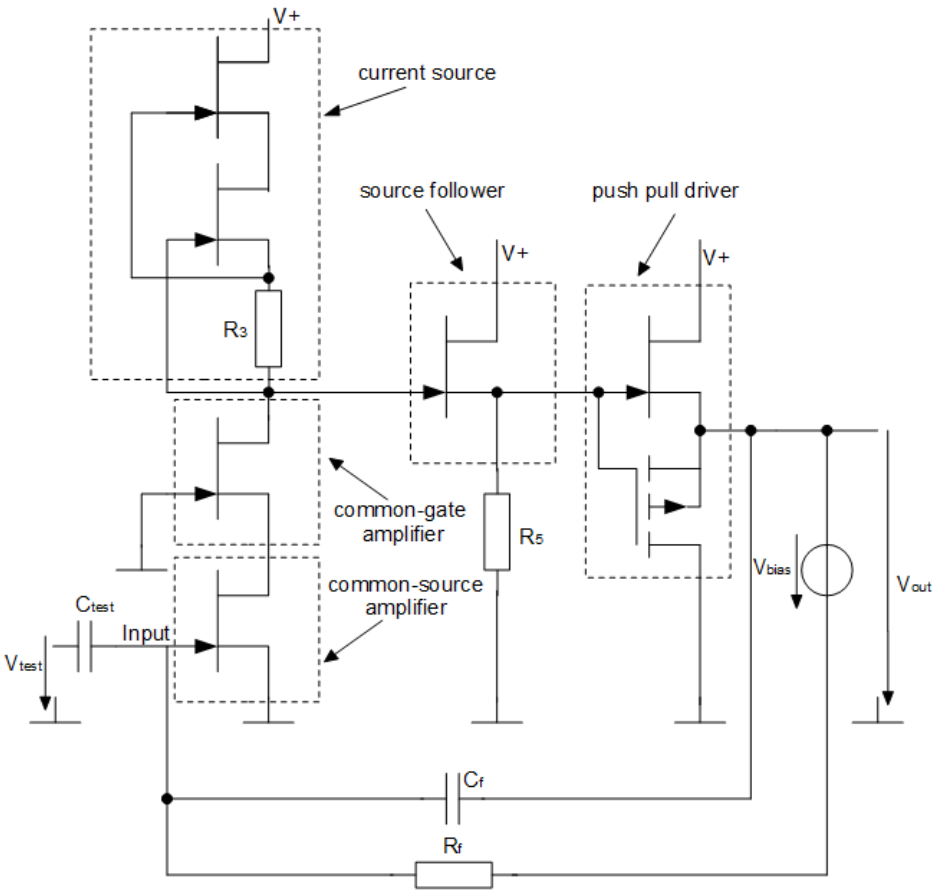

Figure 2.7: Preamplifier circuit, divided into separate components

2.2 Post Amplifier Design

The main purpose of the post amplifier is additional amplification and biasing, the basic design of the post amplifier can be seen in figure 2.8. The amplification is done with an operational amplifiers, one is set as an inverting amplifier and is responsible for dc biasing and amplification, the other operational amplifier is set as a non inverting amplifier and its only purpose is amplification. The FET used in the post amplifier is configured in the common-source configuration with a source resistor, the amplification of this circuit can be calculated with equation 17.

$$A_{S_{RS}} = \frac{-g_m(R_D||r_{out})}{1 + (RV_2||R_8)} \tag{17}$$

r_{out} is usually very large compared to R_D and therefore can be neglected. Equation 17 in addition shows that the amplification can be adjusted by variation of the potentiometer RV_2.

To compensate the amplification and have a pure dc feedback the capacitance C_2 and the resistor R_{10} create a low-pass filter, filtering the feedback. Simulations showed that the circuit oscillated, secondary to the extra phase shift created by C_2, to compensate the phase shift the capacitance C_6 was added, for now with high frequencies the phase shift is practically none existent. For C_2 and R_{10} to still create a low-pass filter C_2 must be much larger then C_6, $C_2 >> C_6$.

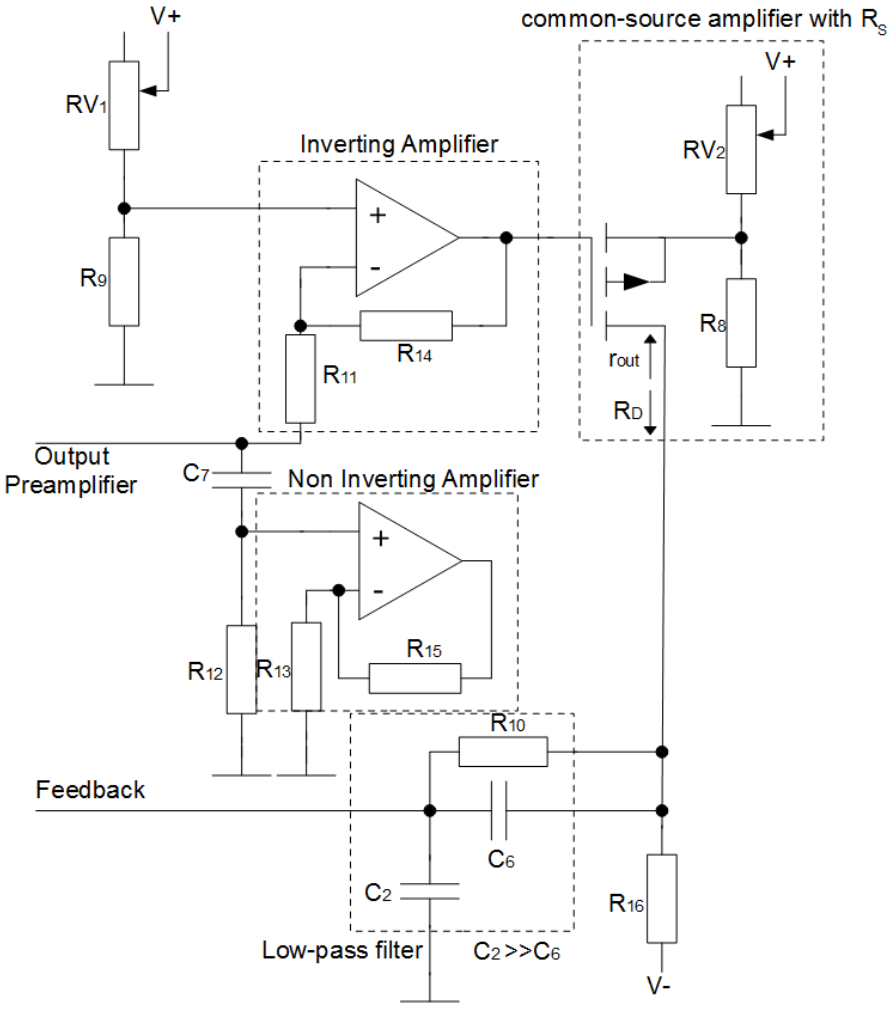

Figure 2.8: Post amplifier circuit, divided into separate components

By adjusting the potentiometer RV_1 the voltage of the positive input of the inverting operational amplifier can be set, the operational amplifier tries to minimize the voltage between its inputs, this results in the negative input having the same dc voltage as the positive input. Therefore the dc voltage of the output of the preamplifier can be adjusted by adjusting the potentiometer RV_1, through the amplification of the FET circuit the output of the inverting amplifier is barely affected by this adjustment. Therefore with adjusting the amplification of the FET circuit the dc voltage at the output of the inverting amplifier can be set. With the output of the amplifier being the output of the inverting amplifier the baseline of the output signal can be adjusted with RV_2.

3 PCB Schematic and Layout

The PCB(Printed Circuit Board) was designed with the software KiCad, and open source project with support from well known institutes such as the University of Grenoble and CERN[9].

The full design with additional soldering pads can be found in section 6 attachments.

3.1 Preamplifier Schematic

Figure 3.1 shows the schematic design of the preamplifier in KiCAD. In addition to the components mentioned in section 2.1 some components were added for purposes of testing. There are two input transistors Q_4 and Q_9 this was done to have multiple footprints for the input transistor, for the SF291 has a TO92 housing and the BF862 has a SOT23 housing, only one of these transistors were soldered in at a time. The resistors R_{20} and R_{19} were added to vary the gate voltage of Q_3, giving the input transistor more drain-source voltage, the purpose of the capacitance C_{17} is to ac ground the gate of Q_3, reducing noise introduced through the additional resistors. The resistor R_6 was added to simulate a coaxial cable, it was replaced by a short when a cable was present between the cut PCB boards.

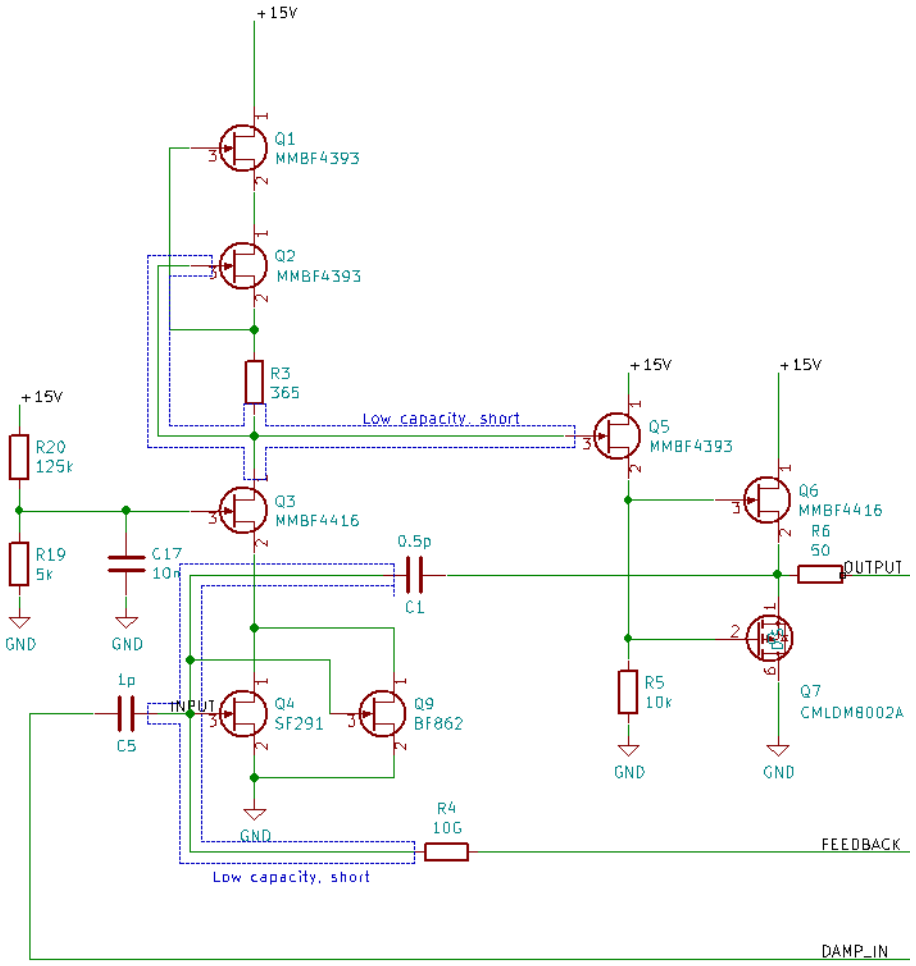

Figure 3.1: KiCad schematic design of preamplifier

All devices were SMD(Surface Mount Devices), and all resistors and capacitances were

available in size 0603 apart from the $0.5pF$ feedback capacitance c_f that was only available in size 0402.

3.2 Post Amplifier Schematic

Figure 3.2 shows the schematic design of the post amplifier in KiCAD. In addition to the components mentioned in section 2.2 some additional components where added. The capacitance C_4 was added to ac ground the positive input of the inverting operational amplifier, to reduce noise. The capacitance C_3 and the resistor R_7 were added to prevent a standing wave when coaxial cable is present between the preamplifier and post amplifier. The considered operational amplifier was the OPA2211 a dual amp operational amplifier, meaning there were two operational amplifiers in one housing. The capacitors C_8 and C_9 were placed very close to the dual amp, filtering the power supplies and for fast demands of energy. The resistors R_1, R_2 and R_{17} create an $\frac{1}{10}$ attenuator for the test signal, with respect to a 50Ω input resistor. This was done to keep the test charge low as mentioned in section 1.2, for reasonable resolution.

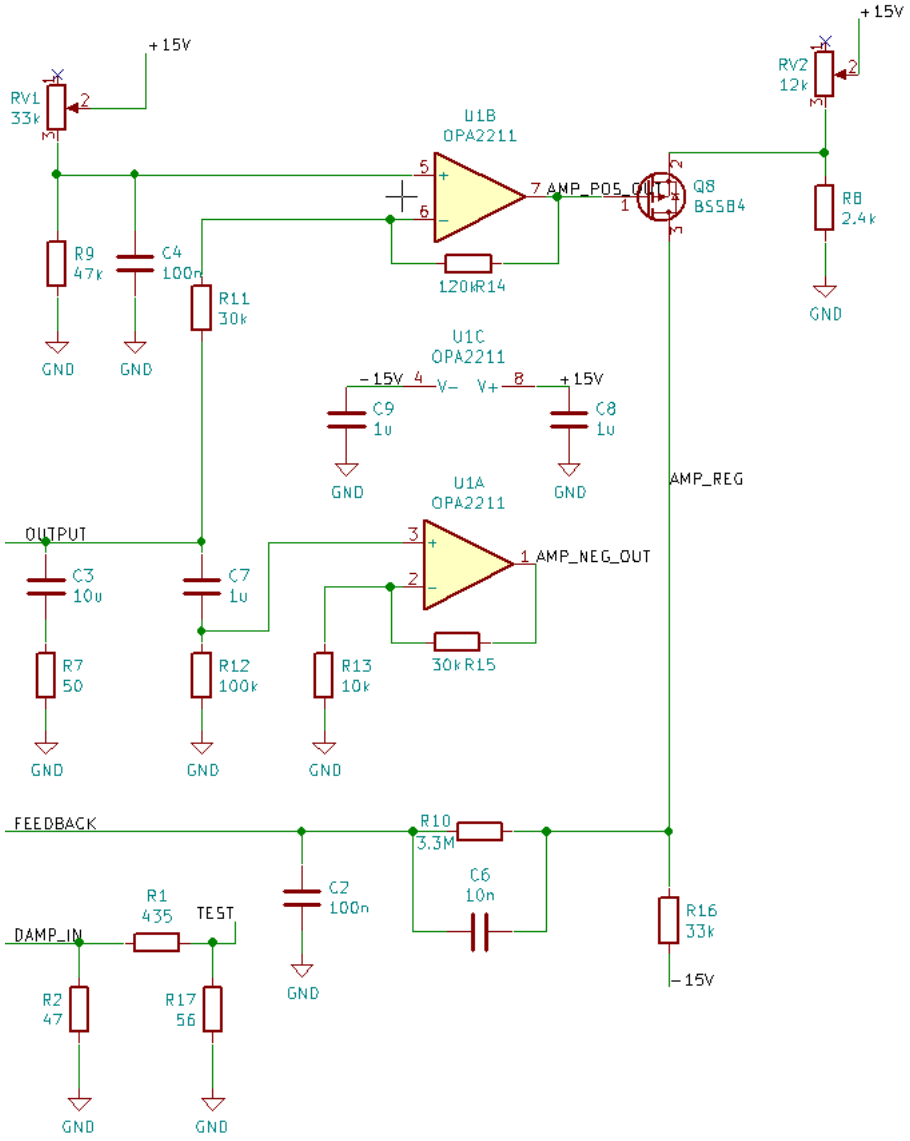

Figure 3.2: KiCad schematic design of post amplifier

All resistor and capacitors were SMD and available in size 0603, apart from the large capacitance C_3, with $10\mu F$ it was only available in size 0805.

3.3 PCB Design

When designing the PCB special care was given to the design of the preamplifier, keeping the input capacitance of the amplifying stage as low as possible, as mentioned in section 1.2 this capacitance has the biggest impact on the noise. Another capacitance that had to be kept low, was the output of the amplifying stage, for this capacitance is responsible for the speed of the amplifier, keeping it low will result in a fast rise time. To keep these capacitors low the connections were kept as short as possible and no ground fill was added to either layer, close to these areas. The stray capacitances introduced through wiring and grounding were measured in section 4.8. The total amount of layers needed for the PCB was two. Figure 3.3 shows a virtual view of the PCB as it can be displayed in KiCAD, some components do not have 3D models and therefore only their footprints appear.

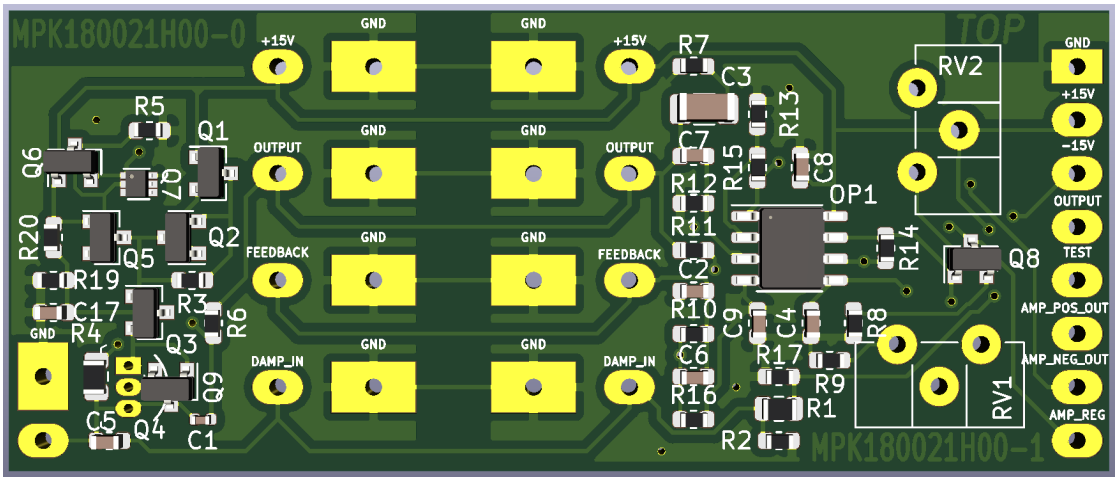

Figure 3.3: KiCad 3D view of PCB

The operational amplifier OPA2211 has an additional pad at the bottom of the IC for better heat dissipation, and was connected to $-15V$ as advised in the data sheet [10]. For easy separation when building an amplifier with multiple meters of cable, additional pads were added to solder the coaxial cable. Large ground pads on which the outer shield could be soldered were placed at the edges of the cutting line, and shortly behind them smaller pads for the core. In addition pads were added for ground, $+15V$, $-15V$, output for the output of the preamplifier, test for test input, and outputs for the operational amplifier AMP_POS_OUT for the inverting operational amplifier and AMP_NEG_OUT for the non inverting operational amplifier, AMP_REG was the drain of FET amplifying stage in the post amplifier. All these soldering pads had vias for better robustness. All layers in more detail can be found in section 6 attachments.

4 Experimental Work and Measurements

All components were soldered on the PCB and a RF housing was build with five BNC connectors, test input, preamplifier output, inverting operational amplifier output and two for power supply in addition a banana socket was added for grounding. Figure 4.1 shows the finished amplifier in its RF housing, with the housing grounded. Isolation was placed under the PCB to prevent the pads on the bottom side from shorting with ground. First tests showed the amplifier was not working with the positive power supply going into the current restriction. Separating the preamplifier from the post amplifier lead to isolating the issue to the preamplifier. After further investigation, it was found that the footprint of Q_7 the CMLDM8002A was for the Japanese version with only the American version being available, this was fixed with some artistic soldering, as can be seen in figure 4.2, and must be corrected in the next design.

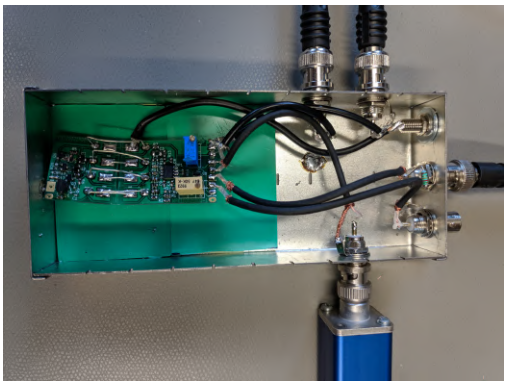

Figure 4.1: Amplifier in RF housing

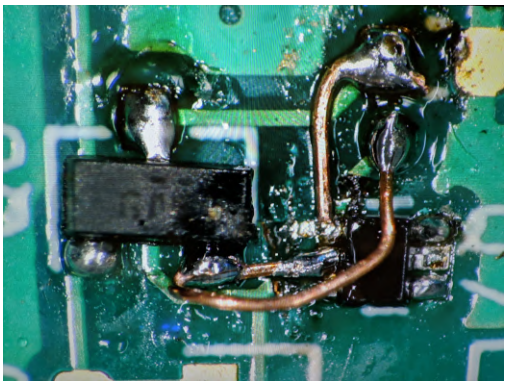

Figure 4.2: Fix for CMLDM8002A layout

The working amplifier had a current draw of $I_{plus} = 16.5mA$ and $I_{minus} = 8.5mA$. The wanted voltages were set by the potentiometer, the output of the preamplifier to $\approx 9V$ dc and the output of the inverting operational amplifier to $\approx 0V$ dc. When measuring the output of the preamplifier, this must be done with capacitive coupling, because of the high dc value, this was done with a $1000\mu F$ capacitance, to construct a high-pass filter with a very low cutoff frequency.

4.1 Power Supply

The initial power supply was two four cell lithium-ion batteries with each $2700mAh$, connected in series to supply $\pm 15V$ with the middle being ground. Both outputs had LC-filters to filter out any additional noise. A three-way switch was build in, first position charging, second off and third on with LC filter. There were two issues found with this design, one being that the resistor of the inductance was very high, this caused the voltage two drop when a Load was connected, in the case with the amplifier the positive supply voltage dropped from $+15.5V$ to $+13.3V$. The second issue was that when switching on the voltage supply, the switch bounces causing multiple high voltage peaks of up to $40V$, figure 4.4 shows the response when turning on the power supply. These high voltage peaks caused the operational amplifier to break which lead to very high current flow causing the PCB track to the operational amplifier to evaporate.

Figure 4.3: Power supply with two lithium-ion batteries

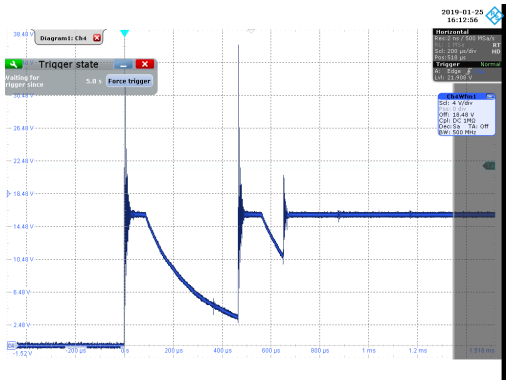

Figure 4.4: Turn on response of power supply

The first response to this issue was soldering two $3300\mu F$ capacitors in the amplifier from each supply current to ground, this was a rather short term solution, for the capacitors were very large and taking away a lot of space in the RF housing and in addition the issue with the supply voltage dropping was not solved.

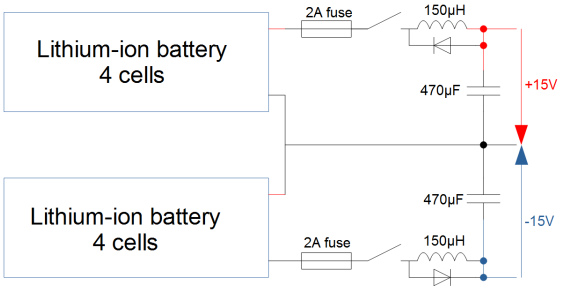

Figure 4.5: Modified power supply setup

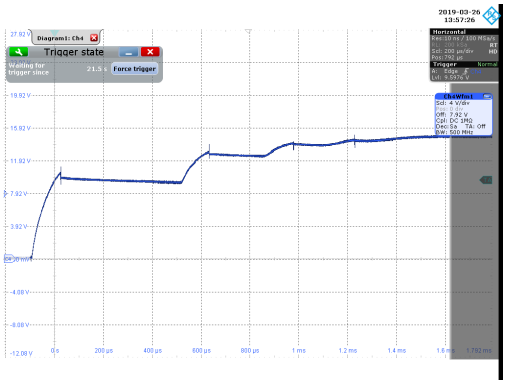

Figure 4.6: Turn on response with LC-filter and diode

The second response was to exchange the the impedance with one with a lower resistance and soldering a flyback diode parallel to the impedance, figure 4.5 shows the updated circuit. The purpose of the flyback diode is to stop the high voltage peaks caused by the switch bouncing and the inductance trying to resist the fast voltage drop causing multiple high voltage peaks. The original design had a resettable fuse or polyfuses, issues with polyfuses are that they are very dependent on temperature and slow. The polyfuses were not removed but in addition to them two melting fuses were added with interrupt ratings of $2A$, these protect from a high discharge and limit the charging current, for the maximum charging current of the lithium ion batteries is $2.7A$. Figure 4.6 shows the turn on response with the modified circuit, one can still see the bouncing of the switch, but the high voltage peaks have been eliminated. The two $3300\mu F$ capacitors were removed, after testing showed no more voltage peaks.

4.2 Rise Time

The rise time is defined as the time for a signal to rise from 10% to 90% of its amplitude. As mentioned in section 3.1 the speed of the preamplifier is dependent of the capacitance at the output, keeping the output capacitance of the common-gate amplifier low will give the amplifier a fast rise time. Therefore the input capacitance of the source follower must

be kept low, the input capacitance of a MMBF4393 is given with a maximum of $14pF$ [11]. As a test Q_5 was removed and the gate-pad was connected to the source-pad, in addition R_5 had to be removed to keep the output impedance of the amplifying stage high. In addition the capacitors C_3 and C_7 were removed to only measure the rise time of the preamplifier without the low-pass filters from C_3 and C_7 . The results of this test can be seen in figure 4.8.

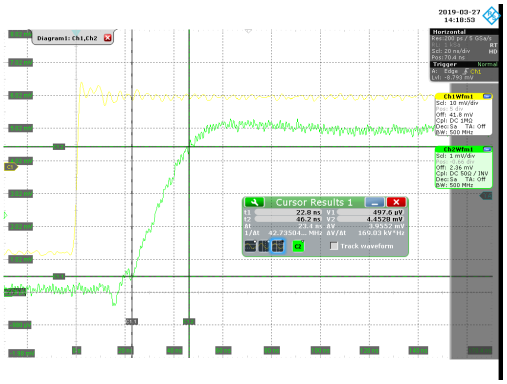

Figure 4.7: Rise time preamplifier with Q_5

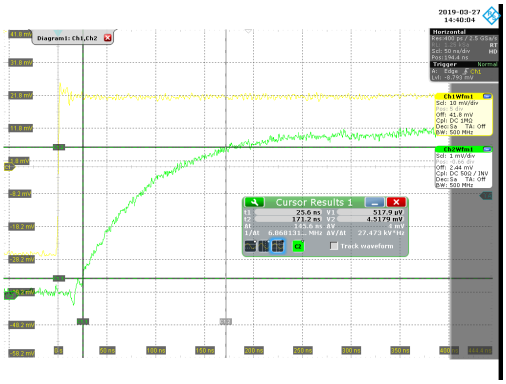

Figure 4.8: Rise time preamplifier without Q_5

Figure 4.7 shows the rise time of the preamplifier with Q_5 and R_5, the resulting rise time is $23.4ns$. When removing Q_5 and R_5 as mentioned above the output capacitance rises, since now the input capacitance of the source follower is replaced by the input capacitance of the push-pull driver. The input capacitance of the push-pull driver is calculated by the input capacitance of a MMBF4416(max. $4pF$ [12]) and parallel the input capacitance of a CMLDM8002A(max. $70pF$ [13]), resulting in a maximum capacitance of $74pF$, making the amplifiers rise time a lot slower as seen in figure 4.8, it rises to $146ns$.

Figure 4.9: Rise time post amplifier

Figure 4.10: Rise time post amplifier with $1pF$ feedback

The next measurement conducted was the speed of the post amplifier, this is dependent on the slew rate of the operational amplifier for the opa2211 it is given with $27\frac{V}{\mu S}$ [10], and therefore the rise time of the post amplifier is dependent on the voltage of the input signal. Figure 4.9 shows the response of a square input signal with a voltage of $50mV_{pp}$. Figure 4.9 also shows that the operational amplifier tends to overshoot, to compensate this overshoot multiple capacitors were soldered parallel to the feedback resistor of the inverting operational amplifier R_{14}. The best results were achieved with a $1pF$ feedback capacitance. Figure 4.10 shows the response signal with a $1pF$ feedback capacitance, with practically no loss of rise time and almost completely compensating the overshoot.

4.3 Operational Amplifier Noise

First measurements of the inverting and non inverting output of the operational amplifier showed that the inverting output had more noise than the non inverting output, this was due to the high resistor values of the inverting operational amplifier, R_{11} and R_{14}. The resistor values were initially chosen high, $R_{11} = 30k\Omega$ and $R_{14} = 120k\Omega$ to minimize the dc current from the preamplifier.

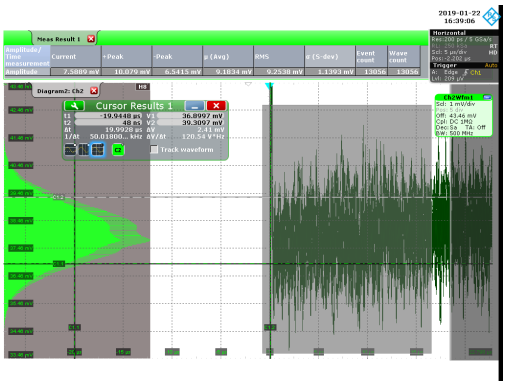

Figure 4.11: Noise measurement of post amplifier with gain resistors $30k\Omega$ and $120k\Omega$

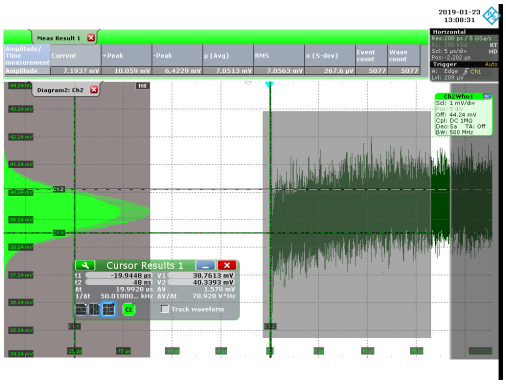

Figure 4.12: Noise measurement of post amplifier with gain resistors $3k\Omega$ and $12k\Omega$

The noise was measured with the histogram function of the RTO1014 oscilloscope from Rhode & Schwarz. The initial noise with $R_{11} = 30k\Omega$ and $R_{14} = 120k\Omega$ was $2.4mV$ FWHM, figure 4.11. The resistors were varied with keeping the ratio $\frac{R_{14}}{R_{11}} = 4$ in mind , table 4.1 shows the results of this measurement.

R_{14}	$120k\Omega$	$30k\Omega$	$12k\Omega$	$1.2k\Omega$
R_{11}	$30k\Omega$	$7.5k\Omega$	$3k\Omega$	300Ω
$FWHM$	$2.4mV$	$1.9mV$	$1.6mV$	$1.6mV$

Table 4.1: Noise measurement of operational amplifier OP2211, with variation of gain resistors

The measurement results show that the noise does not improve with resistors lower than $R_{11} = 3k\Omega$ and $R_{14} = 12k\Omega$, for that reason the resistors were changed, keeping the dc current of the preamplifier and the noise low. For all following measurements $R_{11} = 3k\Omega$ and $R_{14} = 12k\Omega$.

4.4 Drain-Source Voltage

As mentioned in section 2.1 the resistors R_{19}, R_{20} and the capacitance C_{17} were added to variate the gate voltage of Q_3 the FET of the common-gate amplifier, this would lead to the drain-source voltage of the input FET Q_4 to change proportionally. To get a reference of the noise, the histogram function of the oscilloscope was used, briefly mentioned in section 4.3.

R_{20}	$\infty\Omega$	$125k\Omega$	$22k\Omega$	$10k\Omega$
R_{19}	0Ω	$5k\Omega$	$5k\Omega$	$5k\Omega$
V_{G3}	$0V$	$0.6V$	$3.4V$	$5V$
V_{DS4}	$1.8V$	$2.4V$	$5.2V$	6.8Ω
$FWHM$	$395\mu V$	$406\mu V$	$400\mu V$	$405\mu V$

Table 4.2: Noise measurement of preamplifier with variation of drain source voltage of input FET

Table 4.2 shows the results of some noise measurements with variation of the gate voltage of the common-gate amplifier. Taking a small measurement error into account the measurements show that the variation the drain source voltage of the input FET, (here the SF291) practically had no affect on the total noise of the preamplifier.

4.5 Function Generator

The function generator used for testing of the amplifier, was the AFG3252C from Tektronix. A noise measurement of the function generator had to be conducted to conclude its noise attribution in the measurement setup. The noise measurement was done with the RTO1014 oscilloscope from Rhode & Schwarz, it has a measurement setup where the standard deviation of the amplitude can be measured, and directly displayed on the oscilloscope. Multiple measurements showed that the measurement results were affected by the amplitude and time scale of the oscilloscope. When the time resolution was set to high $100\frac{ns}{div}$, the standard deviation was $\sigma = 0V$. This showed that the oscilloscope lost in resolution to realize high sampling rates. To get a sufficient measurement resolution the time scale was set to $200\frac{\mu s}{div}$ and the amplitude scale to $500\frac{\mu V}{div}$. The results showed a standard deviation of $\sigma = 7.6\mu V$ for an amplitude of $\overline{V} = 24mV$. To guarantee that there were a sufficient amount of measurements, and the resolution was high enough, the measurements of the oscilloscope were displayed in a histogram, the resulting resolution was $4\mu V$. The resolution was high enough for the measurement of $\sigma = 7.6\mu V$, with equation 18 the FWHM of the function generator can be calculated.

$$FWHM = 2.35\ \sigma \tag{18}$$

The resulting resolution in Full Width Half Maximum for a test signal of $24mV$ is $FWHM_{FG} = 17.86\mu V$, this is sufficient enough for the Tektronix AFG3252C to be used in noise measurements. With a test signal amplitude of $5mV$ the corresponding $FWHM$ is $3.6\mu V$.

4.6 Operational Amplifier Testing

The first considered operational amplifier was the OPA2211 from Texas Instruments, because of its low noise $1.1\frac{nV}{\sqrt{Hz}}$ at $1kHz$, high speed and the ability to run at $\pm 15V$ with nearly rail to rail output. The OPA2211 was mentioned in [14] to be working at 140k, so still had to be tested for 77k. For this the PCB from section 3 was cut in half and the post amplifier side was modified to fit the circuit seen in figure 4.13. In addition to the devices seen in figure 4.13 two capacitors were soldered from each supply-voltage to ground, as in the original design. The inverting OPA (Operational Amplifier) was wired as in the original post amplifier design, the non-inverting OPA was wired only to prevent it from oscillating, and with a high gain to measure the slew rate.

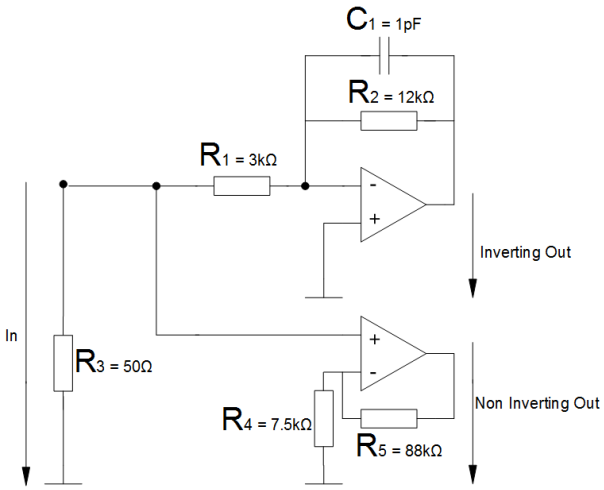

Figure 4.13: Operational amplifier testing circuit

LEMO cables were soldered on to the PCB for input, output signals and power supply $\pm 15V$. The circuit was tested at room-temperature and in liquid nitrogen at $77k$. Figure 4.14 shows the OPA at room-temperature, yellow (top) the input signal, a square wave with an amplitude of $1V$ at $200Hz$, orange (middle) the output signal of the inverting OPA and green (bottom) the output of the non inverting OPA, figure 4.15 shows the equivalent in liquid nitrogen. The measurement results show that the OPA2211 oscillates at $77k$.

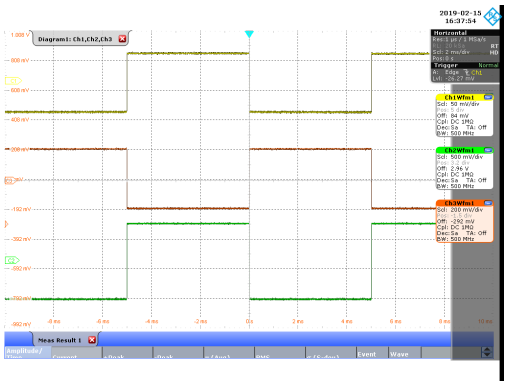

Figure 4.14: OPA2211 at room-temperature

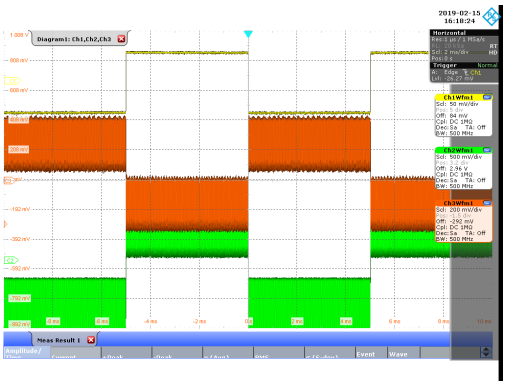

Figure 4.15: OPA2211 in liquid nitrogen at $77k$

Measurements were conducted with multiple feedback capacitors $1pF$, $10pF$ and $47pF$

non reduced the oscillations enough. Multiple supply voltages were tried $\pm 15V$, $\pm 10V$ and $\pm 5V$ non had any effect on the output signals.

The next operational amplifier tested was the AD8066 from Analog Devices. The AD8066 has voltage noise of $7nV\frac{nV}{\sqrt{Hz}}$, a $-3dB$ bandwidth of $145MHz$, a slew rate of $180\frac{V}{\mu s}$ and a maximum supply voltage of $24V$ [15]. Therefore the post amplifier would need some minor modifications if the AD8066 would be the considered operational amplifier. The same circuit was used as for the OPA2211 as seen in figure 4.13.

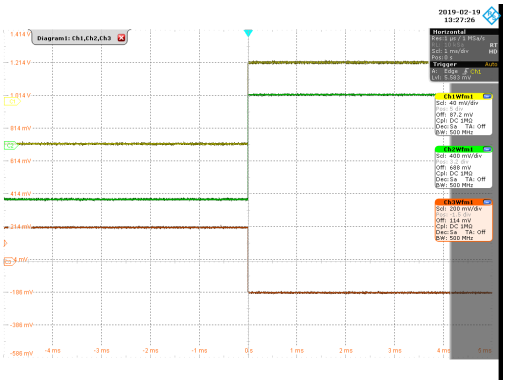

Figure 4.16: AD8066 at room-temperature

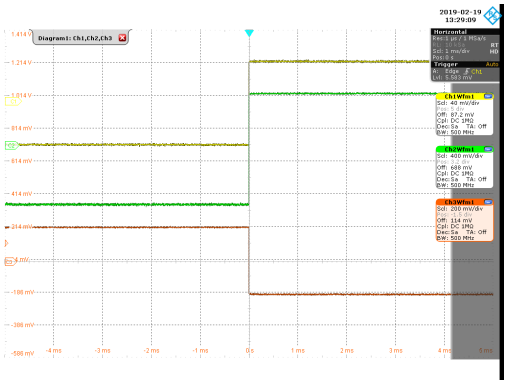

Figure 4.17: AD8066 in liquid nitrogen at $77k$

Figure 4.16 shows the AD8066 at room temperature, and figure 4.17 in liquid nitrogen, no changes can be seen in the output signal and no additional oscillations, showing that the temperature difference had practically no effect on the AD8066.

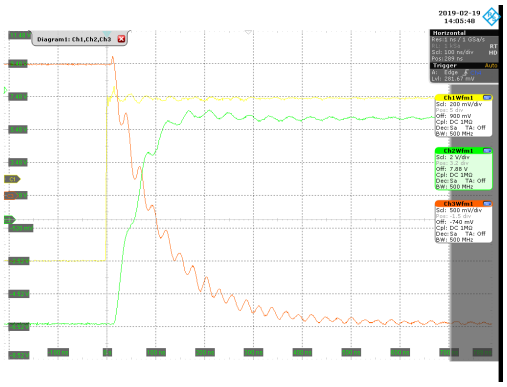

Figure 4.18: AD8066 slew rate measurement at room-temperature

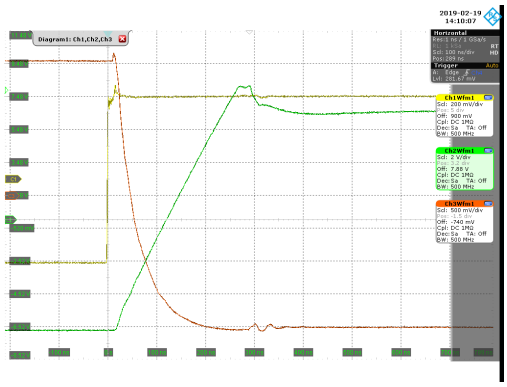

Figure 4.19: AD8066 slew rate measurement in liquid measurement

Figure 4.18 shows the slew rate of the AD8066 at room temperature and figure 4.19 liquid nitrogen, the operational amplifier becomes slower in liquid nitrogen, with the slew rate declining from $180\frac{V}{\mu s}$ to $60\frac{V}{\mu s}$.

4.7 Input FET Noise Measurements

As mentioned in section 3.1 the PCB was designed to house multiple input FETs, the two considered at the time of design was the BF862 from NXP semiconductors and the SF291 from Semefab, during measurements two additional FETs came into consideration the MX-11rc from Moxtek and the BF998 a dual-gate MOSFET from NXP semiconductors. To have a better understanding of which FET was suited best as the Input FET a test circuit was designed to measure the amount of noise in dependency of the current, figure 4.20 shows the test circuit. The FET is in the common-source configuration, with variation of the gate voltage the drain current can be adjusted, the current can be measured by measuring the voltage drop over R_1. The first operational amplifier has an ac gain of ≈ 12 the second operational amplifier has a gain of 1, it was only implemented for the first stage oscillated with a capacitance at the output, or a coaxial cable. With the 50Ω at the output of the second operational amplifier and the 50Ω in the spectrum analyzer the total amplification after the source circuit is ≈ 6, it was measured at $50kHz$ in room temperature with $A_{OP300k} = 5.85$ and in liquid nitrogen $A_{OP77k} = 6.0$. Figure 4.21 shows the modifications that had to be done to fit the BF998. The circuit was implemented on the PCB designed in section 3. Two measurements were conducted, the first being the amplification of the FET and the second a noise measurement of the FET, both with various drain currents.

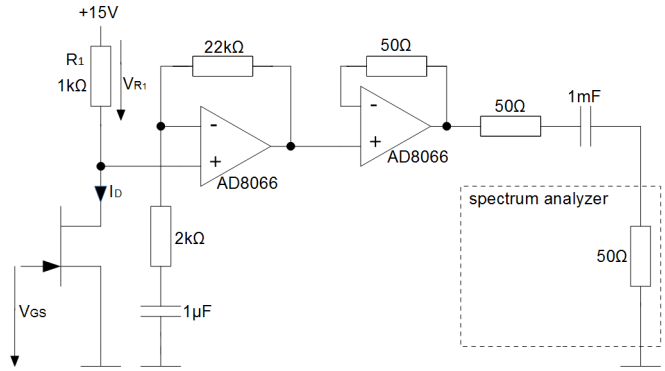

Figure 4.20: Circuit for noise measurement of input FET

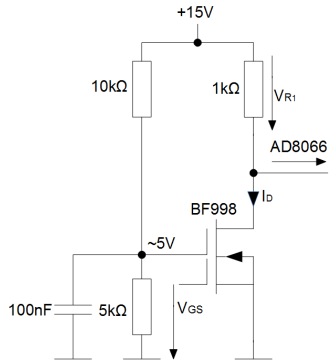

Figure 4.21: Modification for noise measurement with BF998

To measure the amplification of the FET a sine function with an offset was applied to the gate, with variation of the offset the drain current I_D can be adjusted, the function generator used was the AFG3252C from Tektronix. The amplified signal was measured with the RTO1014 oscilloscope, at the drain, with an input impedance of $1M\Omega$.

The second measurement, was a noise measurement of the FET, for this measurement a low-pass filter was added to the input of the FET, lowering the noise input of the function generator. The function generators output signal was set to dc, the voltage drop over R_1 was measured with a digital multimeter, that had to be disconnected when conducting the noise measurement for it contributed a large amount of noise. The noise was measured with a spectrum analyzer from Rhode & Schwarz the FSV7, from $10Hz$ to $100kHz$. The resolution bandwidth (RBW) was set to $1kHz$, the noise was measured in dBm and then calculated with equation 19 to $\frac{nV}{\sqrt{Hz}}$.

$$[\frac{V}{\sqrt{Hz}}] = \sqrt{10^{\frac{[\frac{dBm}{1kHz}]-60dB-A[dB]}{10}} 50\Omega} \tag{19}$$

$$A[dB] = 20log(A_{OP}\ A_{FET}) \tag{20}$$

With $A[dB]$ being the total amplification of the circuit in dB, and $[\frac{dBm}{1kHz}]$ the noise measured in dBm with $RBW = 1kHz$, A_{FET} is the measured amplification of the FET circuit.

Note that some of the noise measurements with $1mA$ in liquid nitrogen were very high, to still have a reasonable graph these traces were divided by a factor mentioned in the legend of the plot, and must be multiplied for the correct noise values.

4.7.1 BF862

The first considered FET was the BF862, with its SOT23 housing it was an easy implementation on the PCB. Its noise was given at $0.8\frac{nV}{\sqrt{Hz}}$ at $100kHz$ with $V_{GS} = 0V$, this would result in $I_D = I_{DSS} \approx 20mA$[16].

I_D	$1mA$	$2mA$	$4mA$	$6mA$	$8mA$	$10mA$
$A_{FET}\ \ T = 300°k$	12	17	22	26	28	29
$A_{FET}\ \ T = 77°k$	12	19	26	31	33	34
V_{DS}	$14V$	$13V$	$11V$	$9V$	$7V$	$5V$

Table 4.3: Amplification of BF862 with variation of current, at room temperature and in liquid nitrogen

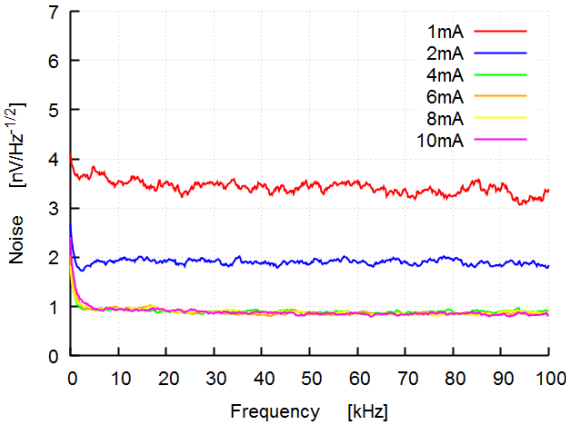

Figure 4.22: Noise measurement of BF862 at room temperature

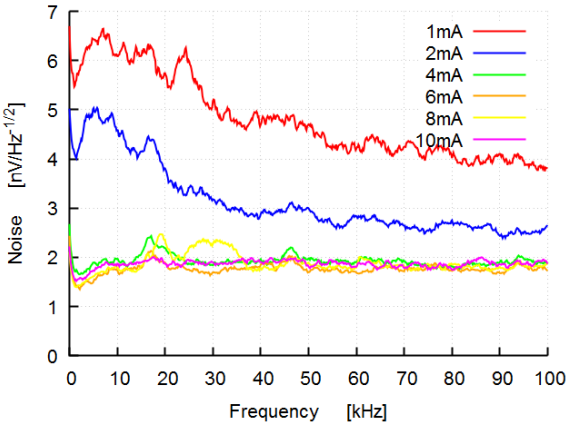

Figure 4.23: Noise measurement of BF862 in liquid nitrogen

The results show that at $100kHz$ the noise is $\approx 0.9\frac{nV}{\sqrt{Hz}}$, the small variation can be explained by part tolerances and that the noise of the spectrum analyzer was not taken into consideration. The BF862 showed practically no improvement above $4mA$, both at room temperature and in liquid nitrogen. By far the BF862 had the best results at $1mA$ in liquid nitrogen, with other FETs having values more than 10 times the amount.

4.7.2 SF291

The SF291 with its TO92 housing was easy to implement on the PCB, for it had a matching footprint. The SF291 was the only FET without any prior given noise information.

I_D	$1mA$	$2mA$	$4mA$	$6mA$	$8mA$	$10mA$
A_{FET} $T = 300°k$	9	12	16	19	20	21
A_{FET} $T = 77°k$	9	14	19	23	25	26
V_{DS}	$14V$	$13V$	$11V$	$9V$	$7V$	$5V$

Table 4.4: Amplification of SF291 with variation of current, at room temperature and in liquid nitrogen

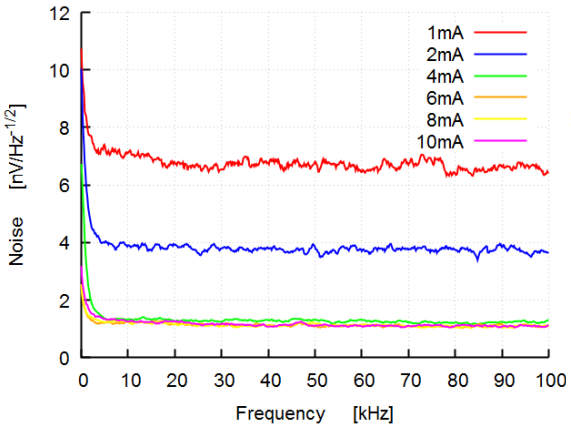

Figure 4.24: Noise measurement of SF291 at room temperature

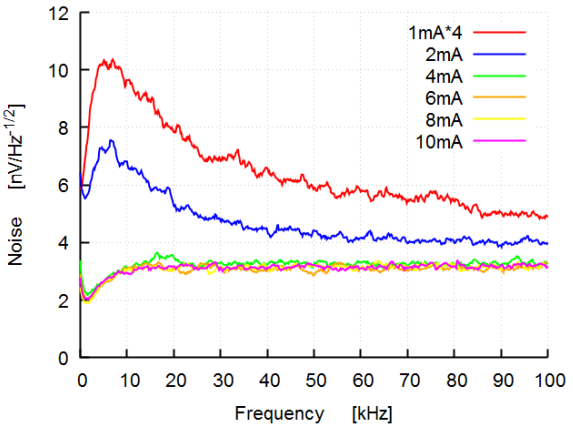

Figure 4.25: Noise measurement of SF291 in liquid nitrogen

The noise measurement at $1mA$ in liquid nitrogen was divided by a factor of 4 for better graphics, and must be multiplied for correct values.

The SF291 showed similar results as the BF862, apart from the SF291 having a very high noise with $1mA$ in liquid nitrogen. Again practically no improvement were seen with currents higher than $4mA$ at room temperature and in liquid nitrogen. The SF291 also showed to have less amplification than the BF862.

4.7.3 MX-11rc

The MX-11rc had a TO-72 housing, and therefore did not have a matching footprint on the PCB, additional wires were soldered to connect the FET, a correct footprint could lead to a small improvement in noise. Its noise was given at $2.1\frac{nV}{\sqrt{Hz}}$ at $100kHz$ with a drain current of $I_D = 5mA$ [17].

I_D	$1mA$	$2mA$	$4mA$	$6mA$	$8mA$	$10mA$
A_{FET} $T = 300°k$	4	5	6	6	7	7
A_{FET} $T = 77°k$	5	7	9	10	10	11
V_{DS}	$14V$	$13V$	$11V$	$9V$	$7V$	$5V$

Table 4.5: Amplification of MX-11rc with variation of current, at room temperature and in liquid nitrogen

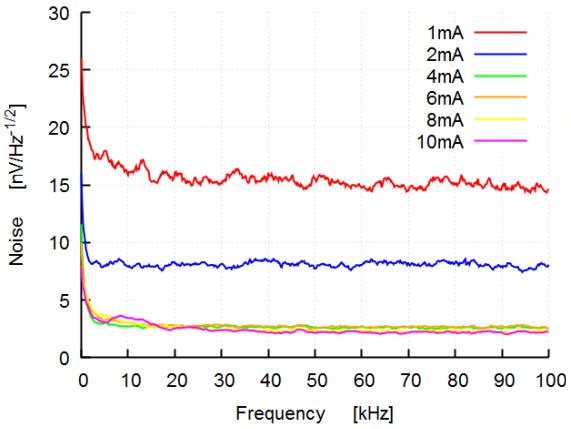

Figure 4.26: Noise measurement of MX-11rc at room temperature

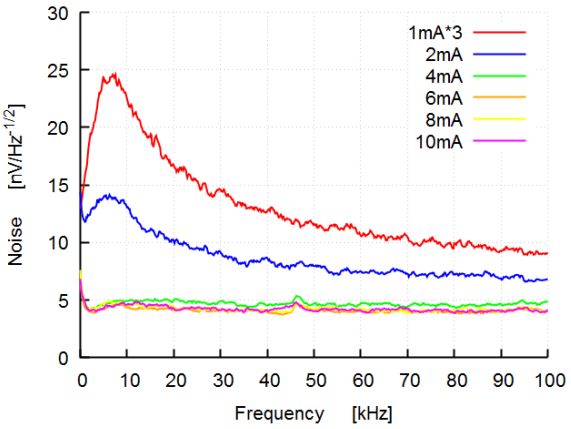

Figure 4.27: Noise measurement of MX-11rc in liquid nitrogen

The noise measurement at $1mA$ in liquid nitrogen was divided by a factor of 3 for better graphics, and must be multiplied for correct values.

The MX-11rc had the highest noise levels at room temperature with $1mA$ and improved by a factor of almost 10 with a current of $4mA$. Again no improvement was seen with currents higher then $4mA$, with a minimum of $\approx 2\frac{nV}{\sqrt{Hz}}$ at $100kHz$, which is a good match to the given data. The MX-11rc as the SF291 showed very high noise at $1mA$ in liquid nitrogen reaching up to $70\frac{nV}{\sqrt{Hz}}$.

4.7.4 BF998

As mentioned in section 4.7 the BF998 needed some modifications to fit the designed circuit, these modifications were shown in figure 4.21, with $gate_1$ as the input and $gate_2$ at $5V$, with ac grounding. With $gate_2$ at $5V$ the current was limited and measurements were only done with a maximum of $4mA$. There was no matching footprint for the BF998 which needed additional wiring to connect it, a matching footprint could lead to a small improvement in noise. The BF998 had no prior given noise information [18].

I_D	$1mA$	$1.5mA$	$2mA$	$3mA$	$4mA$
A_{FET} $T = 300°k$	7		10	12	14
A_{FET} $T = 77°k$	8	11			
V_{DS}	$14V$	$13.5V$	$13V$	$12V$	$11V$

Table 4.6: Amplification of BF998 with variation of current, at room temperature and in liquid nitrogen

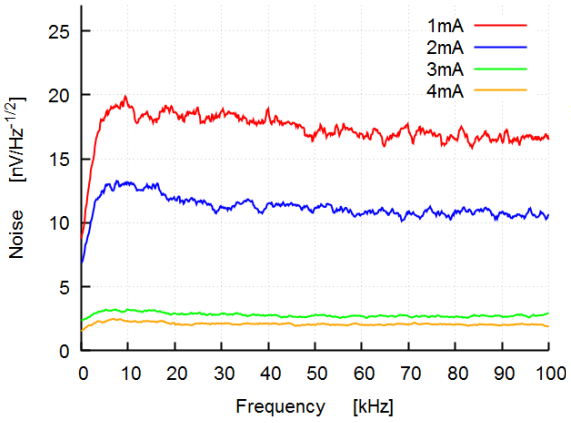

Figure 4.28: Noise measurement of BF998 at room temperature

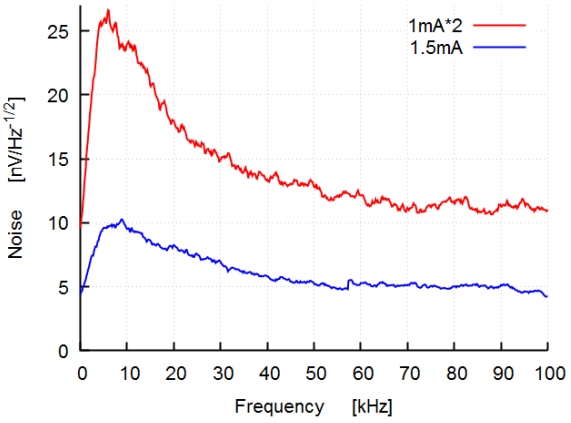

Figure 4.29: Noise measurement of BF998 in liquid nitrogen

The noise measurement at $1mA$ in liquid nitrogen was divided by a factor of 2 for better graphics, and must be multiplied for correct values.

The BF998 showed similar results to the other tested FETs, with $4mA$ it reached $\approx 2\frac{nV}{\sqrt{Hz}}$ at $100kHz$. The BF998 had a high shift if threshold voltage when placed into liquid nitrogen, this needed a positive gate voltage for drain currents higher then $1mA$ and limited it to a maximum of $1.6mA$. This makes the BF998 practically unusable at cold temperatures, for with $1.5mA$ it reaches a voltage noise $\approx 5\frac{nV}{\sqrt{Hz}}$ at $100kHz$, which is more than twice as high as all other tested FETs, with their max currents.

The best voltage noise was measured with the BF862, which had similar results to the SF291, with currents highers then $1mA$. The MX11-rc had noise voltage with a factor two higher than the Bf862 and Sf291, nevertheless the MX11-rc has a very low input capacitance of $0.7pF$ [17] which could lead to a noise drop in the finished setup. The BF998 turned out to be practically unusable at cold temperatures.

All FETs showed an increase in noise in liquid nitrogen, to eliminate that the noise increase was coming from the operational amplifier the noise measurement circuit was modified to measure the noise of the operational amplifier, figure 4.30 shows the modifications. The input of the AD8066 was set to $5V$ and ac grounded to minimize the noise of the resistors. The noise was measured as in previous measurements, with the exception that the amplification of the FET from equation 19 was set to 1, $A_{FET} = 1$. The given noise of the AD8066 according to its data sheet was $7\frac{nV}{\sqrt{Hz}}$.

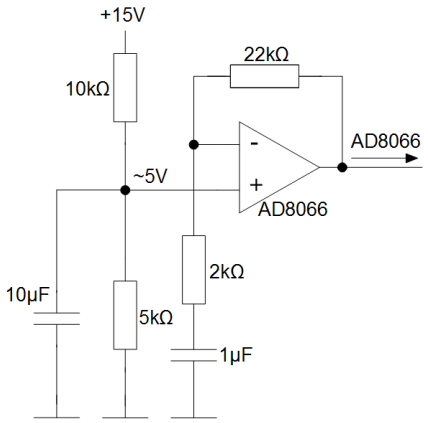

Figure 4.30: Modification of circuit to measure noise of AD8066

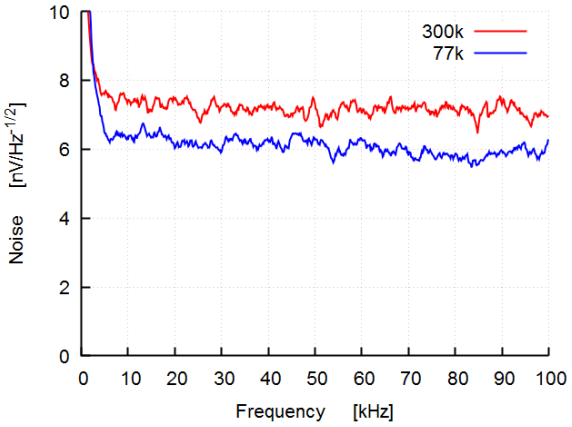

Figure 4.31: Noise measurement of AD8066

The Measurement results of the AD8066 can be seen in figure 4.31, they show that the given noise and measured noise match very well, with approximately $6\frac{nV}{\sqrt{Hz}}$ at room temperature. The noise of the AD8066 improved slightly when placed into liquid nitrogen, with approximately $6\frac{nV}{\sqrt{Hz}}$. This measurement excludes the AD8066 from introducing additional noise, when placing the test circuit in liquid nitrogen.

In addition to all measurements being reliant on the noise of the AD8066, the $1k\Omega$ at the drain of the FET also contributes to all measurements, for the current is measured by measuring the voltage drop over the resistor. If this resistor would drastically change its value when placed into liquid nitrogen the corresponding current would be wrong. To exclude this the resistor was soldered to two wires and the resistance was measured at room temperature and in liquid nitrogen, the results showed 995Ω at room temperature and 1000Ω in liquid nitrogen. This measurement eliminates the error that the measured current is wrong in liquid nitrogen.

4.8 Calibration of Capacitance

As mentioned in section 1.2 the capacitance C_5 or C_{test} is used to have a reference of the amount of charge injected into the amplifier, therefore the exact value of the capacitance is important, and relies on all resulting measurements. Even if using a capacitance with very low tolerances a capacitance is added, for the layout and the soldering pads have a capacitance. When the input capacitance is only $1pF$ these capacitors are not negligible. Equation 21 shows the gain of the preamplifier, with respect to parasitic capacitances.

$$\frac{\hat{V}_{out}}{\hat{V}_{test}} = \frac{C_5 + C_{layout1}}{C_1 + C_{layout2}} \tag{21}$$

Soldering in a capacitance with $22pF$ as the test capacitance C_5 reduces the influence of parasitic capacitors by a factor of 22, making them practically negligible. Five different $22pF$ capacitors were soldered in to compensate tolerances, the gain was measured and averaged over all capacitors. If now the $1pF$ capacitance is soldered back as the test capacitance the ratio between the the amplification with $1pF$ and $22pF$ can better determine the actual test capacitance. If the input signal is the same for both tests, a more exact value can be calculated for the test capacitance with equation 22.

$$\frac{\hat{V}_{out22pF}}{\hat{V}_{out1pF}} = \frac{85.65mV}{5.06mV} = \frac{22pF + C_{layout1}}{1pF + C_{layout1}} \approx \frac{22pF}{1pF + C_{layout1}} \tag{22}$$

$$1pF + C_{layout1} \approx \frac{22pF \;\; 5.06mV}{85.65mV} = 1.29pF \tag{23}$$

$$C_{layout1} \approx 0.29pF$$

With the better determined test capacitance the amplification can be corrected, with a resulting amplification of $24\frac{keV}{mV}$, for a test signal of $5mV$ the corresponding charge would be $120keV$. With the known stray capacitance of the test capacitance $C_{layout1}$, the stray capacitance of the feedback capacitance $C_{layout2}$ can be calculated with equation 22, resulting in $C_{layout2} \approx 0.14pF$.

4.9 Measurements Setup for Noise Measurement

The Flash ADC GERDA system is a flash ADC for data sampling combined with a VME computer for data processing, it was used for the measurements of the GERDA collaboration, and is used for the following noise measurements. To use the Flash ADC GERDA system a measurements setup had to constructed, figure 4.32 shows the setup. Equipment such as the power supply and function generator have been discussed in section 4.1 and section 4.5, respectively.

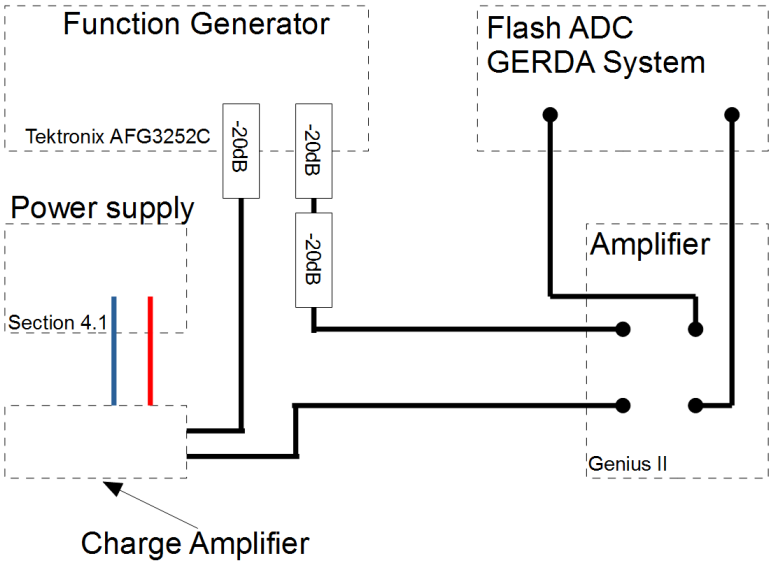

Figure 4.32: Measurement setup with Flash ADC GERDA system

The step test signal generated by the function generator was immediately connected to a attenuator of $-20dB$, assuming the function generator had a constant noise factor that was independent from the amplitude of the output signal, the attenuator would reduce this voltage noise by a factor of 10. From there the signal went into the charge amplifier where it was additionally reduced by a factor of 10. The output of the charge amplifier was connected to a additional amplifier, to reduce the noise of the ADC. The Genius II amplifier is a simple simple operational amplifier setup with an adjustable amplification and dc output. The output of the Genius II amplifier was sampled by the flash ADC and processed by the GERDA system. All cables used coaxial cables to shield the signal from additional RF noise, they were all previously tested.

To have a measure of the noise introduced by components other then the charge amplifier, the same chain was build up without the charge amplifier, with two $-20dB$ attenuators to have the equivalent signal amplitude. The amplification of the Genius II amplifier was adjusted till both output signals had the same amplitude. This signal was also sampled by the flash ADC and processed by the GERDA system. The noise measured for the component other then the charge amplifier was approximately $180eVFWHM$, this noise can be statistically subtracted from the noise measured with the charge amplifier.

The GERDA system to process the data shapes the input signal with a trapezoidal filter and measures the peak position, this peak position is displayed in a histogram, from which the $FWHM$ can be estimated. The filters shaping time can be changed in the source code.

Figure 4.33 shows the measurement system, special care had to be taken with grounding, for it reduced the noise. A large copper rail was added with thick wiring for grounding,a banana socket was added to the charge amplifier for grounding and each coaxial was grounded with a clip the LAN of the VME computer was removed, and the noise was further reduced.

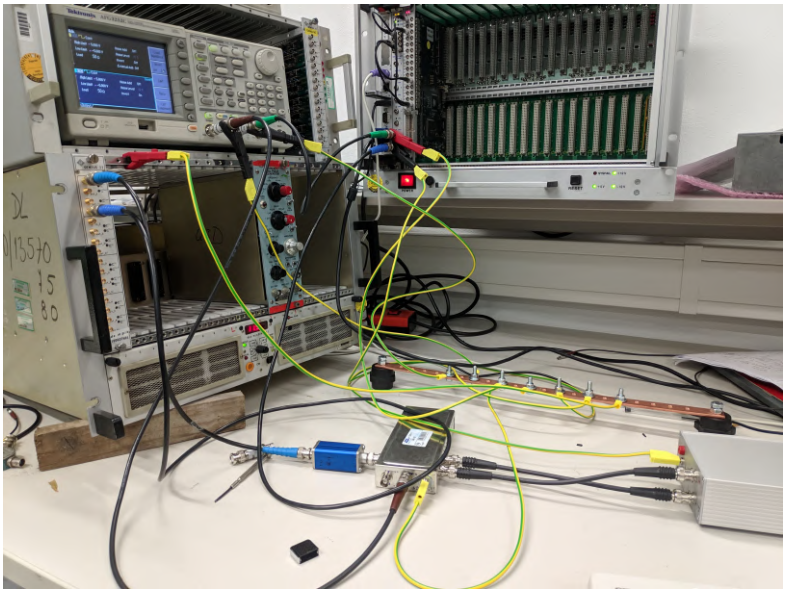

Figure 4.33: Measurement system with Flash ADC GERDA system

Noise is a gaussian function, therefore if the charge amplifier is only affected by noise the histogram will be gaussian, if a non random signal is present in the measurement system the histogram will not be gaussian. Especially supply voltages introduces noise (e.g $50Hz$) creating multiple peaks in the histogram, improved grounding reduced these noise sources.

4.10 Amplifier with Cable

As mentioned in section 3.1 the preamplifier and post amplifier would be separated by a few meters of cable, with the OPA2211 not working in liquid nitrogen, the only possible configuration with this setup would be to separate the preamplifier and post amplifier with 10m of cable. The cable used was a 50Ω RG178 single shielded coaxial cable. Figure 4.34 shows the separated amplifiers in their RF housing. Figure 4.35 shows the preamplifier in its RF housing, additional holes were drilled for easy diving in liquid nitrogen. All cables were 10m long, $+15V$, preamplifier output and feedback, only the test signal input was kept at 1.5m cable length.

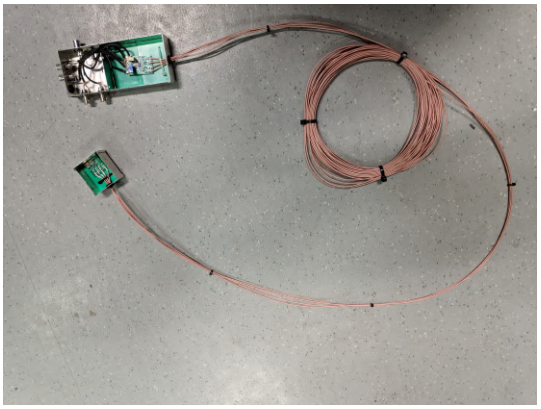

Figure 4.34: Amplifier with 10m coaxial cable

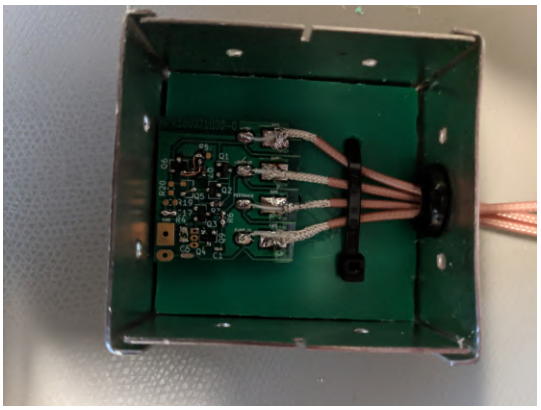

Figure 4.35: Preamplifier with 10m coaxial cables

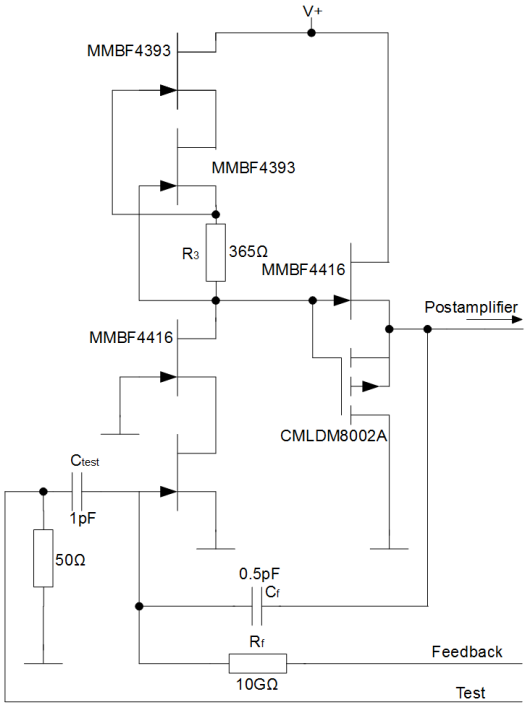

Figure 4.36: Preamplifier circuit layout modifications

With the cables installed between the amplifiers, some minor modifications to the circuit had to be done, figure 4.36 shows the modified circuit. The first modification was adding a 50Ω resistor to the input, preventing reflection, of course the resistors in the post amplifier had to be adjusted to keep the 10:1 attenuation. Figure 4.37 and figure 4.38 show the rise-time of the preamplifier at room temperature and in liquid nitrogen, respectively. The measurement was conducted with the RTO1014 oscilloscope, it showed that the rise-time rose from $23nS$ without the cable to $398nS$ with the cable, at room-temperature. Figure 4.38 shows that by placing the preamplifier in liquid nitrogen the rise-time changes to $364nS$, making it faster in liquid nitrogen. Removing the source-follower had no effect on rise time, and was therefore removed for all following measurements. These measurements were done with the SF291 as the input FET.

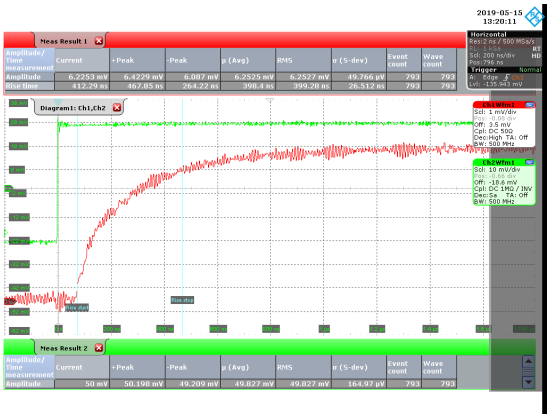

Figure 4.37: Rise time measurement of amplifier with cable at room temperature

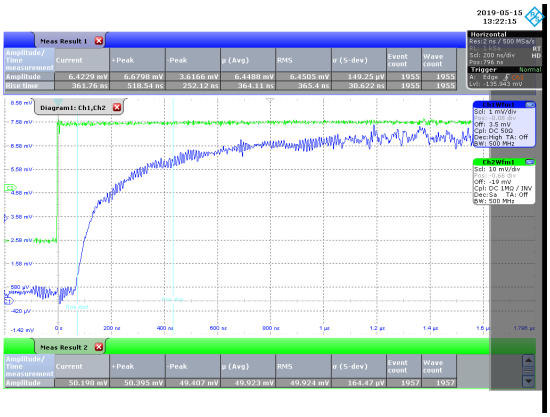

Figure 4.38: Rise time measurement of amplifier with cable in liquid nitrogen

4.11 Noise Measurement of Amplifier with Cable

As in section 4.7 multiple input FETs were measured, here in the amplifier circuit with cable. The noise was measured in FWHM with the FlashADC GERDA system detailed in section 4.9. The measurements were conducted at room temperature and in liquid nitrogen, by placing only the preamplifier in liquid nitrogen. The shaping time was varied from $1\mu s$ to $50\mu s$ with single steps from $1\mu s$ to $10\mu s$, and measurements at $15\mu s$, $20\mu s$ an $50\mu s$. The measurement points were fit to equation 24 using the nonlinear least-square (NLLS) Marquardt-Levenberg algorithm.

$$Q_n[FWHM] = \sqrt{a\tau + \frac{b}{\tau} + c} \tag{24}$$

The noise is then divided into its opponents a parallel noise, b series noise and c for the $\frac{1}{f}$ noise. Initial fits showed negative components, and the equation had to be modified to equation 25.

$$Q_n[FWHM] = \sqrt{|a|\tau + \frac{|b|}{\tau} + |c|} \tag{25}$$

With the modification of the equation, no more negative components were present. The noise was measured by approximately adjusting two cursors to the half of the maximum and measuring the $FWHM$, some issues developed with this approach, nonlinearities were introduced by the ADC causing the peak to not be clearly recognizable, this resulted in a substantial variance during measurements.

4.11.1 BF862

The BF862 was soldered in as Q_9, and Q_4 was removed making the BF862 the only input FET. The resistor R_3 was 365Ω as in the initial design, and this resulted in a drain current for the input stage of $2.6mA$ at room temperature and $\approx 2mA$ in liquid nitrogen.

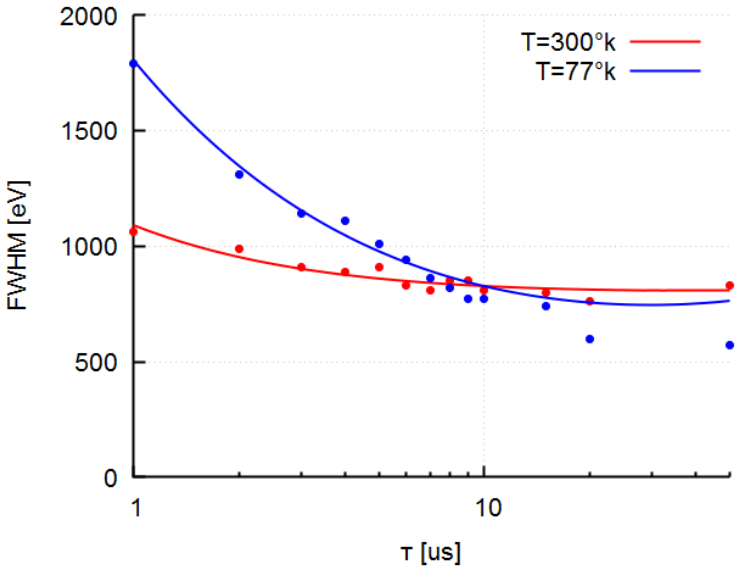

Figure 4.39: Noise measurement of amplifier with 10m of coaxial cable and BF862 as the input FET

	$T = 300°k$	$T = 77°k$
a	331	$3.2\ 10^3$
b	$565\ 10^3$	$2.9\ 10^6$
c	$624\ 10^3$	$360\ 10^3$

Table 4.7: Noise parameters with BF862

The BF862 showed a large increase in noise for low shaping times when placed into liquid nitrogen, this can be partial explained with the decrease in rise time, leading to a higher bandwidth, and therefore introducing more noise. This increase in noise as expected decreased for larger shaping times where the noise was less than at room temperature. Nevertheless the rise time only decreased by approximately 10% not explaining the increase in noise of approximately 60%. As expected there was practically no parallel noise, for no detector was present and the gate current is very low, and decreased when placed into liquid nitrogen. The $\frac{1}{f}$ noise was least effected by the temperature difference.

4.11.2 SF291

The BF862 was removed from Q_9 and the SF291 was soldered on Q_4, making it the only input FET. The drain current of the input stage was not change and stayed at the initial $2.6mA$ at room temperature and $\approx 2mA$ in liquid nitrogen.

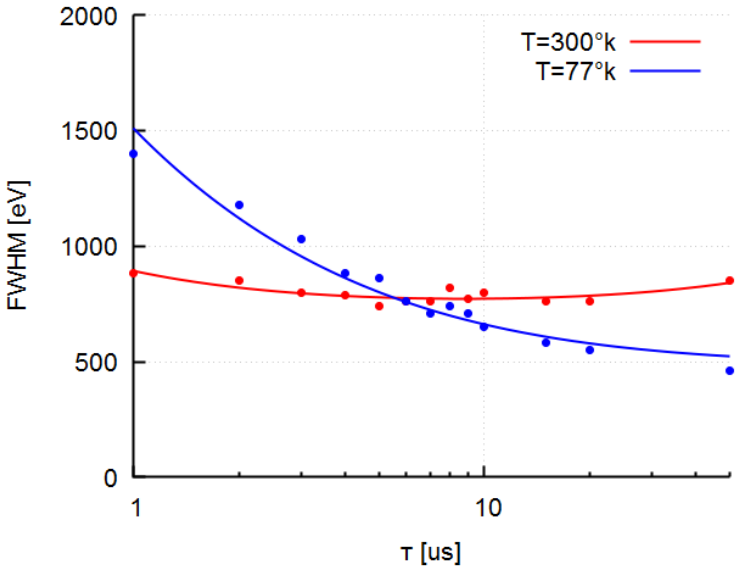

Figure 4.40: Noise measurement of amplifier with 10m of coaxial cable and SF291 as the input FET

	$T = 300°k$	$T = 77°k$
a	$3.2\ \ 10^3$	0
b	$255\ \ 10^3$	$2.0\ \ 10^6$
c	$538\ \ 10^3$	$232\ \ 10^3$

Table 4.8: Noise parameters with SF291

The SF291 showed similar results as the BF862 with a large increase in noise, at small shaping times, when placed into liquid nitrogen, this once again can be partially explained by the increase in bandwidth. The noise decreased for larger shaping times, where less noise was present when the preamplifier was placed into liquid nitrogen, once again practically no parallel noise was present. The SF291 had slightly less $\frac{1}{f}$ noise than the BF862 both in liquid nitrogen and at room temperature, which resulted in the SF291 having less noise than the BF862 for all shaping times.

4.11.3 MX-11rc

The SF291 was removed from Q_4 and the MX11-rc was soldered on Q_4, making it the only input FET. The drain current of the input stage was not changed and stayed at the initial $2.6mA$ at room temperature and $\approx 2mA$ in liquid nitrogen.

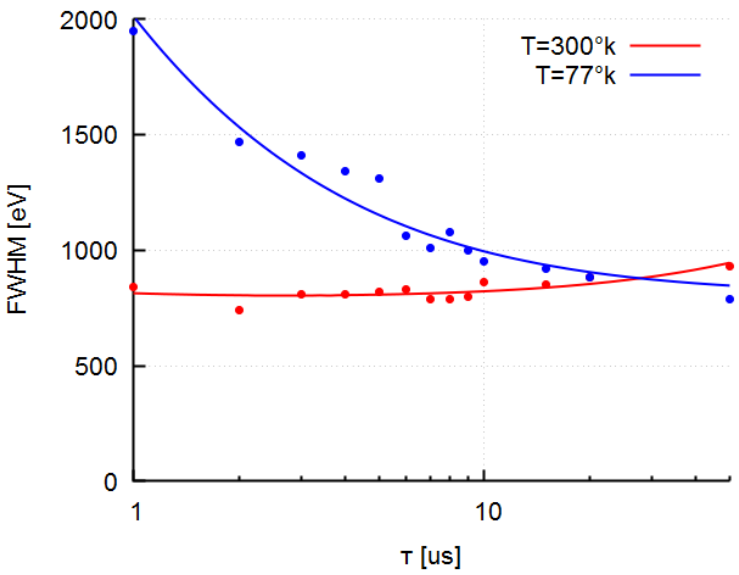

Figure 4.41: Noise measurement of amplifier with 10m of coaxial cable and MX-11rc as the input FET

	$T = 300°k$	$T = 77°k$
a	$5.5\ 10^3$	0
b	$40\ 10^3$	$3.4\ 10^6$
c	$616\ 10^3$	$648\ 10^3$

Table 4.9: Noise parameters with MX-11rc

The MX11-rc showed a similar response as the SF291 and the BF862, with a large increase in noise for low shaping times, when placed into liquid nitrogen. This noise decreased for larger shaping times, where the noise in liquid nitrogen was better then at room temperature. Nevertheless the noise of the MX11-rc was higher than the BF862 and SF291.

4.11.4 BF998

To use the BF998 as the input FET some modification had to be done, Q_4 and Q_3 were removed and replaced by the BF998. The right footprint was not available and additional wiring was needed. The second gate of the BF998 g_2 was soldered to $5V$ and ac grounded as seen in figure 4.42.

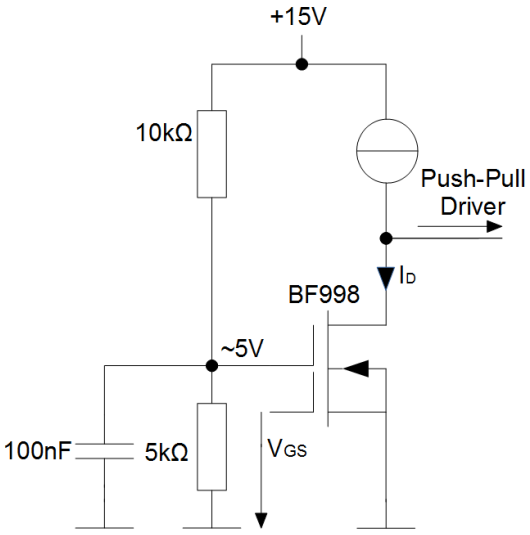

Figure 4.42: Modification of preamplifier for BF998

Measurements in section 4.7 showed that the BF998 had a maximum drain current of $\approx 1.6mA$ in liquid nitrogen, therefore the drain current had to be adjusted. Replacing R_3 with a 680Ω resistor resulted in a drain current of $1.3mA$ at room temperature and $\approx 1mA$ in liquid nitrogen.

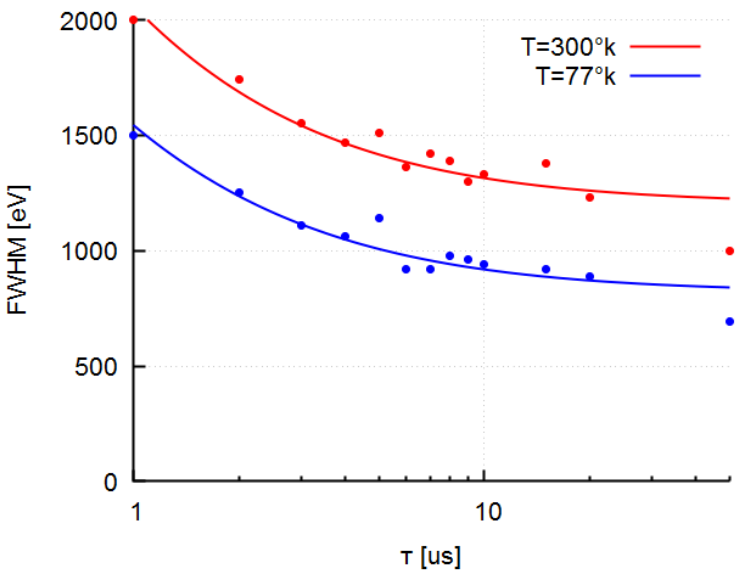

	$T = 300°k$	$T = 77°k$
a	0	0
b	$1.44\ 10^6$	$1.7\ 10^6$
c	$2.8\ 10^6$	$672\ 10^3$

Table 4.10: Noise parameters with BF998

Figure 4.43: Noise measurement of amplifier with 10m of coaxial cable and BF998 as input FET

Measurements with the BF998 were the only measurements, where the noise improved in liquid nitrogen for all shaping times, it improved by a constant of approximately $500eV$.

Again practically no parallel noise was present with out a detector. Nevertheless the noise values with the BF998 were higher then with the BF862 and SF291.

Measurements showed the best noise results, when the SF291 was used as the input FET, therefore some additional modifications were made to the input stage to see if the noise could be further optimized.

4.11.5 SF291 with Bias Resistor

The measurements in section 4.7 showed that the noise of a FET improves with higher drain currents. To keep all FETs of the input stage in the saturation region, only the current of the input FET was raised. This was done by adding a $2k\Omega$ resistor from $+15V$ to the drain of the input FET, this way an additional current given by equation 26 is added to the drain current. The modifications of the circuit can be seen in figure 4.44, in addition to the added resistor the gate of the common-gate amplifier was set to $+5V$ and ac grounded, to give the input FET more drain source voltage and keep it in the saturation region.

$$I_{D2} = \frac{15V - V_{DS_{SF291}}}{2k\Omega} \tag{26}$$

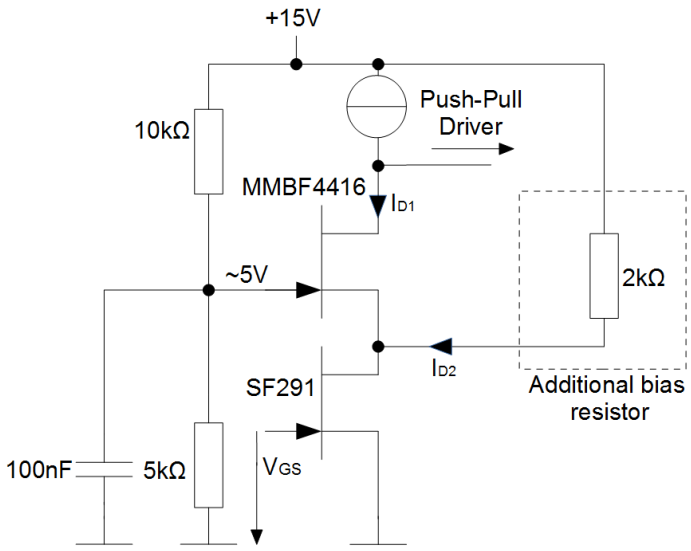

Figure 4.44: Modification of preamplifier for SF291 and added bias resistor

The drain current I_{D1} stayed at the initial $2.6mA$ at room temperature and $\approx 2mA$ in liquid nitrogen. The Drain voltage of the SF291 was at $6.4V$ at room temperature and shifted to $6.2V$ in liquid nitrogen, this resulted in a total drain current for the input FET of $I_{D_{300k}} = 6.9mA$ at room temperature and $I_{D_{77k}} \approx 6.4mA$ when placed into liquid nitrogen.
Figure 4.45 shows the measurement results, showing similar results as without the additional resistor. This could be explained, that with the additional resistor the drain current increases, but the output impedance of the common-source amplifier decreases, this would explain no improvement in noise values. The noise increased for small shaping times when placed into liquid nitrogen, but decreased for large shaping times where the noise values were better then at room temperature.

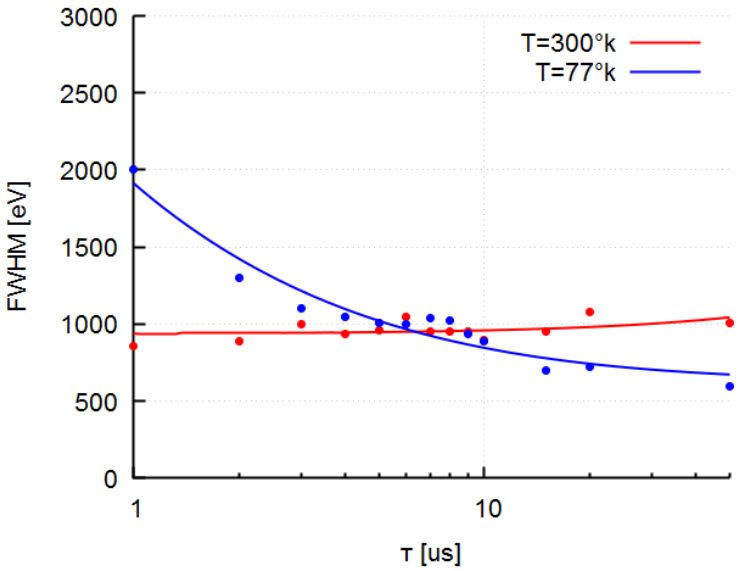

	$T = 300°k$	$T = 77°k$
a	$4.2\ 10^3$	0
b	0	$3.2\ 10^6$
c	$878\ 10^3$	$387\ 10^3$

Table 4.11: Noise parameters with SF291 and additional $2k\Omega$ resistor for biasing

Figure 4.45: Noise measurement of amplifier with 10m of coaxial cable and SF291, with additional $2k\Omega$ resistor

4.11.6 SF291 with additional Current Source

To give the input FET additional drain current but not affect the output impedance of the first amplifying stage the circuit from figure 4.44 was adjust to figure 4.46, where the additional bias resistor was replaced by a current source. This configuration would lead to a increase in drain current without a loss in output impedance of the common-source amplifier.

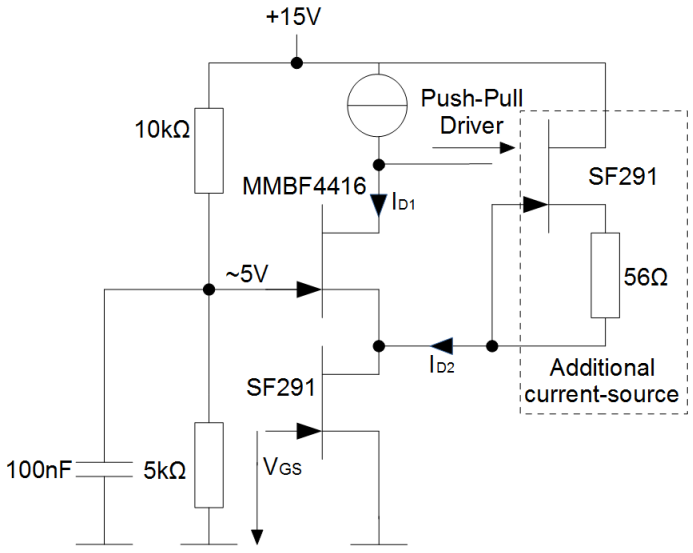

Figure 4.46: Modification of preamplifier, with additional current source

The FET used for the current source was a SF291, with 56Ω resistor between gate and source the resulting drain current was $I_{D2_{300k}} = 10mA$ at room temperature and $I_{D2_{77k}} = 8mA$ when placed into liquid nitrogen, this results in a total drain current for the input FET of $I_{D_{300k}} = 12.6mA$ at room temperature and $I_{D_{77k}} \approx 10mA$ when placed into liquid nitrogen.

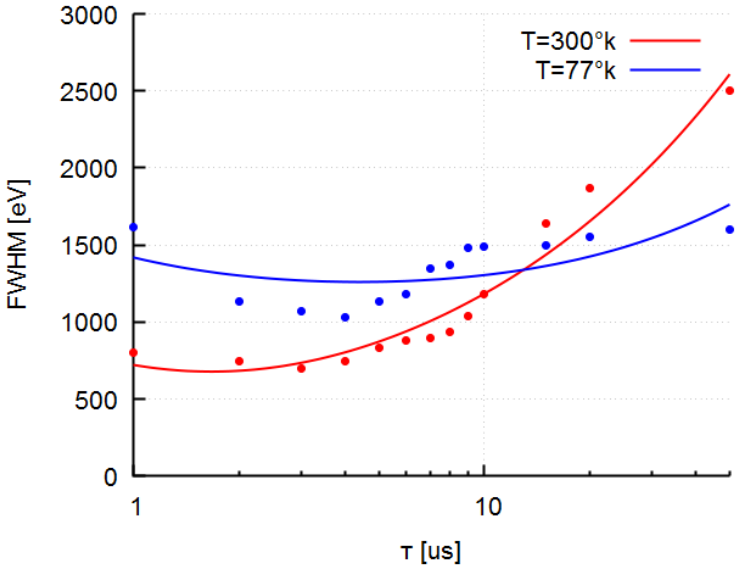

	$T = 300°k$	$T = 77°k$
a	135 10^3	36.5 10^3
b	378 10^3	713 10^6
c	7.1 10^3	1.2 10^6

Table 4.12: Noise parameters with SF291 and additional current source

Figure 4.47: Noise measurement of amplifier with 10m of coaxial cable, the SF291 as the input FET and an additional current source

The results of this measurement were very surprising, for the noise values increased largely, and this was the first measurement with reasonable parallel noise.

4.11.7 SF291 with increased Drain Current

With the noise values not improving with an additional resistor or an added current source, the additional current source was removed and the current of the current source was raised by replacing the resistor R_3 with a 150Ω resistor. The corresponding current was $5.3mA$ at room temperature and $\approx 4.8mA$ in liquid nitrogen.

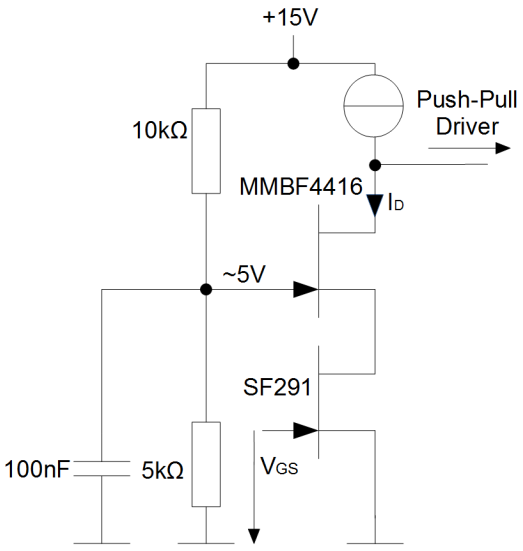

Figure 4.48: Modification of preamplifier, for measurement with increased drain current

Figure 4.48 shows the modifications for the measurements with increased drain current. The gate of the common-gate amplifier was kept at $5V$ to keep the input FET in the saturation region.

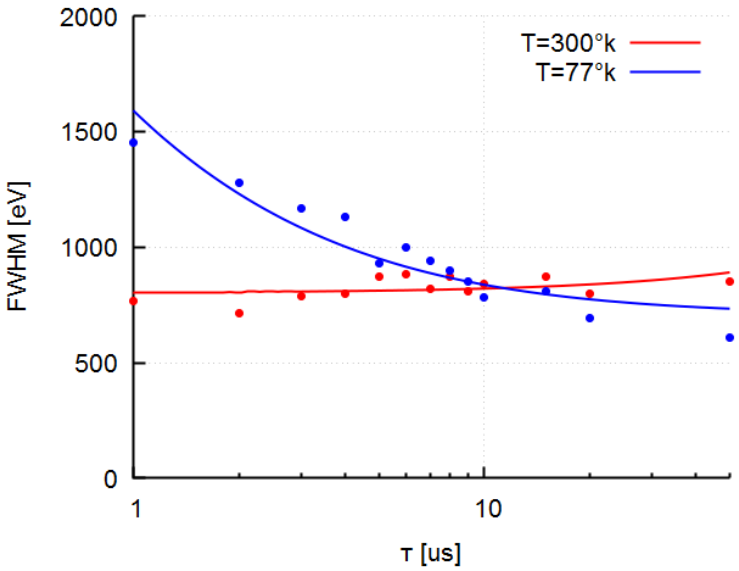

Figure 4.49: Noise measurement of amplifier with coaxial cable and SF291, and increased drain current

	$T = 300°k$	$T = 77°k$
a	$2.9\ \ 10^3$	0
b	0	$2.0\ \ 10^6$
c	$643\ \ 10^3$	$497\ \ 10^3$

Table 4.13: Noise parameters with SF291 and increased drain current

The measurements showed similar results as with smaller current, but there was a small increase in noise. The small increase in noise could be explained by equation 16 describing the open loop gain of the amplifying stage. Equation 27 shows a description of g_m, where K is a constant dependent on the FET, this equation is missing the influence of V_{DS}, but is sufficient enough for higher V_{DS}.

$$g_m = 2\sqrt{K\ \ I_{D0}} \tag{27}$$

Combining equation 16, 27 and 11, gives a function for the open loop gain in dependence of the drain current I_{D0}.

$$A_0 = \frac{v_{out}}{v_{in}} \approx r_{01} r_{02} g_{m1} g_{m2} = \frac{1}{\lambda_1 I_{D0}} \frac{1}{\lambda_2 I_{D0}} 2\sqrt{K_1\ \ I_{D0}}\ \ 2\sqrt{K_2\ \ I_{D0}} \tag{28}$$

Equation 28 shows that $A_0 \sim \frac{1}{I_{D0}}$, this could explain the small increase in noise for larger drain currents, the open loop gain of the amplifier decreases with the increase of drain current.

4.11.8 SF291 with Modeled Detector

The least noise was measured when the SF291 was used as the input FET and the drain current was set to $2.6mA$ at room temperature and $\approx 2mA$ in liquid nitrogen. To better model the effect of detector at the input of this preamplifier, the preamplifier was modified to the circuit seen in figure 4.50. The resistor R_3 of the current source was soldered back to 365Ω, resulting in the initial drain currents, the gate of the common-gate amplifier was set to ground and a capacitance C_{det} was added between input and ground to model the capacitance of a detector.

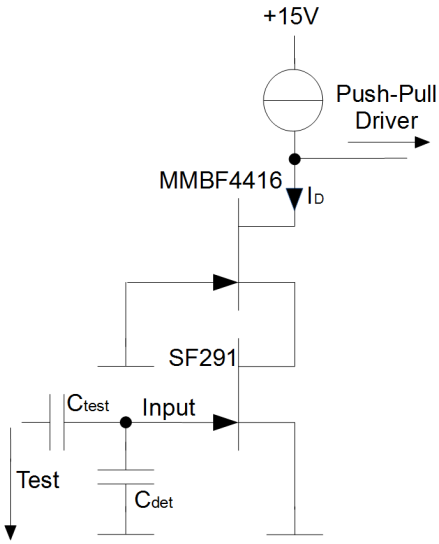

Figure 4.50: Modification of preamplifier, for measurement with modeled detector capacitance

The capacitances of detectors vary from a few picofarad to approximately 20 picofarad, to best cover this range two capacities were tested one with $10pF$ and one with $22pF$. The first measurement conducted was with a $10pF$ capacitance.

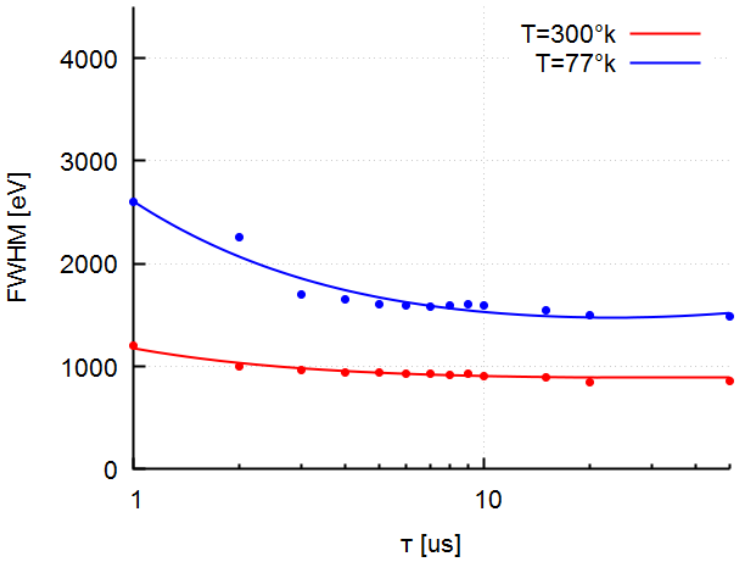

Figure 4.51: Noise parameters with the SF291 as the input FET and a $10pF$ detector capacitance

	$T = 300°k$	$T = 77°k$
a	609	$9.4\ 10^3$
b	$753\ 10^3$	$5.0\ 10^6$
c	$632\ 10^3$	$1.7\ 10^6$

Table 4.14: Noise parameters with SF291 and a $10pF$ detector capacitance

Figure 4.51 shows the results of the noise measurement with a $10pF$ detector capacitance. As expected, the results show an increase in noise, nevertheless the noise in liquid nitrogen is now larger for all shaping times. A possible explanation for the noise in liquid nitrogen constantly being large then at room temperature could be that the capacitance of $10pF$ has a large shift when placed into liquid nitrogen, and is therefore larger than $10pF$.

The $10pF$ detector capacitance was replaced with a $22pF$ capacitance and the measurement was repeated.

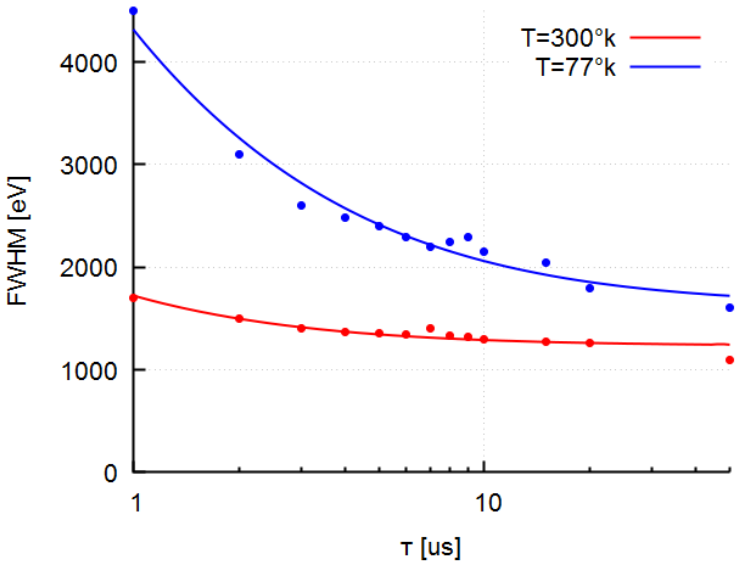

Figure 4.52: Noise parameters with the SF291 as the input FET and a $22pF$ detector capacitance

	$T = 300°k$	$T = 77°k$
a	0	0
b	$1.4\ \ 10^6$	$16.0\ \ 10^6$
c	$1.52\ \ 10^6$	$2.64\ \ 10^6$

Table 4.15: Noise parameters with SF291 and a $22pF$ detector capacitance

Figure 4.52 shows the results of the noise measurement with a $22pF$ detector capacitance. The results show as expected a larger increase in noise compared to a $10pF$ capacitance. Once again the noise level is higher in liquid nitrogen for all shaping times, which once again supports the assumption that the capacitance of $20pF$ rises, when placed into liquid nitrogen.

To better examine the effect of a detector capacitance, without the changes introduces through large temperature variation, the noise measurements with different detector capacitances were plotted with their corresponding temperatures. For clearer graphics only the fit functions are shown.

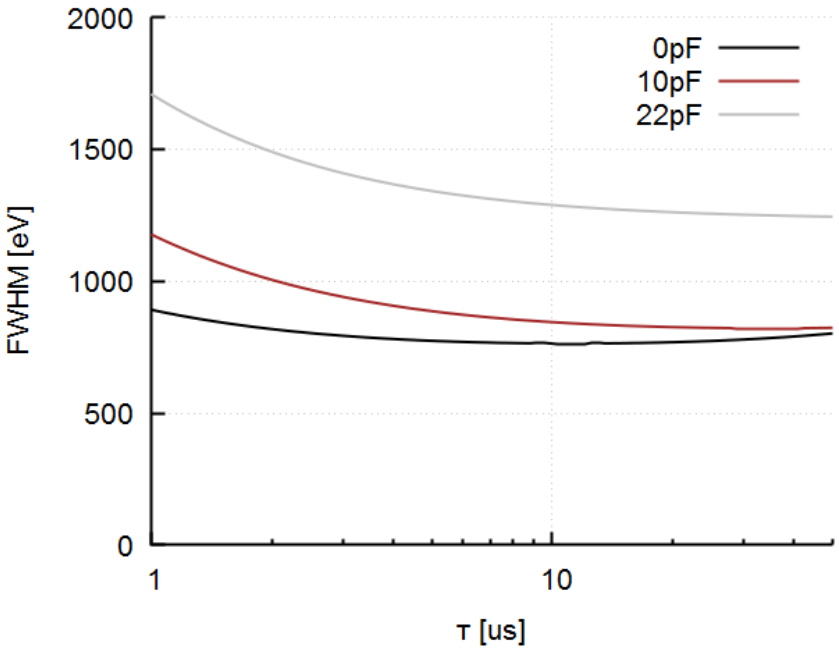

Figure 4.53: Noise measurement with variation of detector capacitance at room temperature

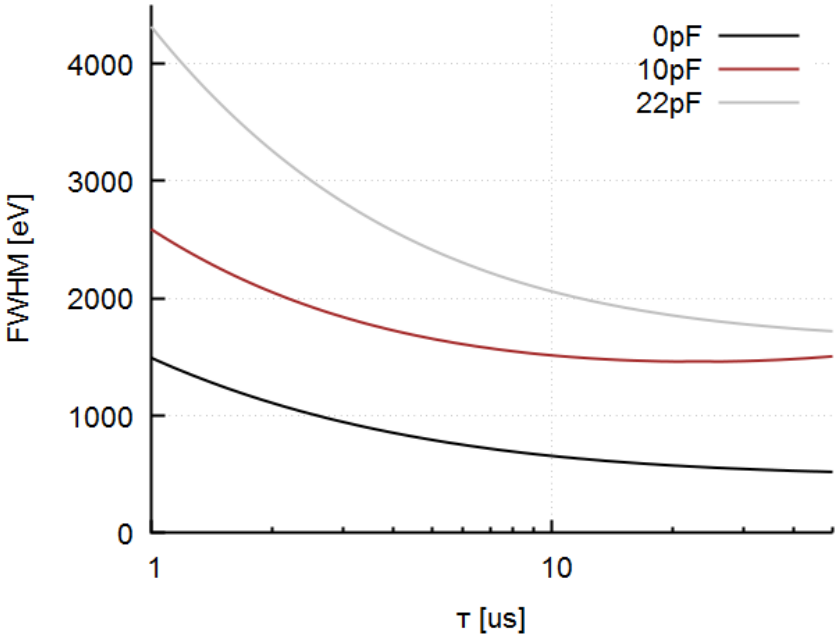

Figure 4.54: Noise measurement with variation of detector capacitance in liquid nitrogen

The noise levels at room temperature with a $10pF$ detector capacitance barely increased, raising the capacitance to $22pF$ on the other hand showed a large increase in noise. When the preamplifier was in liquid nitrogen this increase was more linear.

C_{det}	$0pF$	$10pF$	$22pF$
a	$3.2\ 10^3$	609	0
b	$255\ 10^3$	$753\ 10^3$	$1.4\ 10^6$
c	$538\ 10^3$	$632\ 10^3$	$1.52\ 10^6$

Table 4.16: Noise parameters with modeled detector at room temperature

C_{det}	$0pF$	$10pF$	$22pF$
a	0	$9.4\ 10^3$	0
b	$2.0\ 10^6$	$5.0\ 10^6$	$16.0\ 10^6$
c	$232\ 10^3$	$1.7\ 10^6$	$2.64\ 10^6$

Table 4.17: Noise parameters with modeled detector in liquid nitrogen

in liquid nitrogen this increase was more linear.
Table 4.16 and 4.17 show the noise parameters of the amplifier with a modeled detector, divided into its component, a for parallel noise, b for series noise and c for $\frac{1}{f}$ noise. The parallel noise can be neglected for there are not enough measurements at high shaping times, to have a representative value. Section 1.2 showed that the series noise and $\frac{1}{f}$ noise would rise with a higher input capacitance, this is the case, but once again there are not a sufficient amount of measurements to calculate the relation of noise and the detector capacitance. Nevertheless it gives a reasonable representation for the noise level with a detector added. In addition to a capacitance a detector also has a dark current, therefore the parallel noise would increase when an actual detector would be connected, the noise levels from a shaping time of $5\mu S$ to about $10\mu S$ would practically not be affected by this additional parallel noise, and therefore give a representative value.

5 Discussion

In summary, after a brief introduction into low noise charge amplifiers, there was a detailed explanation of one possible low noise charge amplifier that was assembled into two sections a preamplifier, connected directly to the detector and a post amplifier, assembled away from the detector and connected with a few meters of coaxial cables. Special attention was given to the preamplifier for it is the noise giving component of the amplifier. A PCB was designed, with attention to the noise giving areas, and the circuit implemented. Measurements followed, and minor modification were made to improve noise and rise time.

The input FET is responsible for the majority of the circuits noise, therefore a test circuit was designed and implemented to measure the noise contribution through the FET. Measurements were conducted at multiple drain currents, at room temperature and in liquid nitrogen. All FETs showed higher noise levels in liquid nitrogen. Measurements were taken to investigate if the noise contribution was from other sources such as the operational amplifier, the measurements showed no increase in noise when placed into liquid nitrogen. The best results were reached with the BF862 at $100kHz$, it had a noise level of $2\frac{nV}{\sqrt{Hz}}$ in liquid nitrogen, followed by the SF291 with a slightly higher noise level.

Measurements of power supplies and function generators followed, to build a low noise measurement setup, equipment not meeting the noise requirements was either replaced or modified, till a low noise measurement setup was guaranteed. This measurement setup was implemented with a Flash ADC running the GERDA software, and all noise sources were monitored during measurements.

Further testing showed that the OPA2211 for which the post amplifier was designed, did not work in liquid nitrogen, this meant that the only possible configuration was mounting the post amplifier outside the cryostat. An amplifier with ten meters of coaxial cable was built, measurements indicated a large increase rise time and noise. The noise was eliminated by the data processing of the GERDA software where no difference was measured with or without the cable. The noise of this amplifier was measured with low noise measurement setup, at room temperature and with placing the preamplifier in liquid nitrogen. All measurements were done by varying the filters shaping time implemented in the GERDA software, from $1\mu s$ to $50\mu s$. With the assistance of numerical approximation methods the noise could be divided into three components, series noise, parallel noise, and $\frac{1}{f}$ noise. This helped better narrow down the main noise sources. Multiple input FETs were tested with the amplifier, including the BF998 a dual-gate MOSFET, best results were showed by the SF291 with $FWHM = 500eV$ for high shaping times, it was closely followed by the BF862. Additional modifications where added for biasing (e.g current source, increasing drain current) to try improve the noise measured with SF291, nevertheless all modifications lead to an increase in noise rather than a decrease. The best results with the SF291 as the input FET, therefore measurements followed with a modeled detector, showing the noise effect by adding a detector capacitance. These measurements were done with a $10pF$ and $22pF$ capacitance, representing realistic detector capacitances. The noise measured was approximately in the same range of other designed charge amplifiers.

The main advantages of this charge amplifier compared to others [2] is the minimal construction, low power and self biasing. The minimal design of only six FETs and two resistors for the preamplifier, enables a very small implementation size, that can

be constructed directly at the detector. The low noise preamplifier runs with a power consumption of less than $50mW$, at low temperatures and therefore minimal power is needed for cooling, and a large amount of detectors can be used with minimal heat dissipation. The self biasing of the input FET is the main advantage compared to other charge amplifiers, it enabled the input FET to be replaced with other FETs, and no additional modifications are needed, in addition the preamplifier works with a high feedback resistance of $10G\Omega$, others amplifiers did not work with a feedback resistor higher then $1G\Omega$.

Future improvements of the amplifier is a new design of the post amplifier, for the OPA2211 did not work at low temperatures and the post amplifier had to be mounted outside the cryostat, with a alternative operational amplifier, the post amplifier could also be placed at low temperatures this could lead to an additional improvement of the noise. In addition the ADC sampling of LEGEND will be implemented with differential inputs, therefore the preamplifier will need modifications in the output stage, without changes in the amplifying stage. A alternative that could lead to a reduction in noise is that the preamplifier could be modified to a reset amplifier, this would need a FET acting as a switch, and the large feedback resistor could be removed, which could be responsible for some of the noise. With a FET the high input impedance of the preamplifier would still be satisfied, nevertheless the self biasing of the preamplifier would have to be implemented in another way and would lead to an almost completely new design.

References

[1] N. Abgrall *et al.*, "The large enriched germanium experiment for neutrinoless double beta decay (legend)," *AIP Conference Proceedings*, vol. 1894, no. 1, p. 020027, 2017. [Online]. Available: https://aip.scitation.org/doi/abs/10.1063/1.5007652

[2] S. Riboldi, C. M. Cattadori, A. D'Andragora, A. Pullia, F. Zocca, M. Barnabe-Heider, and D. Budjas, "A low-noise charge sensitive preamplifier for ge spectroscopy operating at cryogenic temperature in the gerda experiment," 12 2010, pp. 1386 – 1388.

[3] [Online]. Available: https://www.mpi-hd.mpg.de/gerda/physics.html

[4] J.-F. Loude, "Energy resolution in nuclear spectroscopy," 2000.

[5] M. Agostini *et al.*, "Results on neutrinoless double beta decay of 76 ge from gerda phase i," 2013. [Online]. Available: https://pure.mpg.de/rest/items/item_1849853/component/file_1849852/content

[6] M. Salathe, "Study on modified point contact germanium detectors for low background applications," 2015.

[7] P. Horowitz and W. Hill, *The art of electronics; 3rd ed.* Cambridge: Cambridge University Press, 2015.

[8] Siliconix, "The fet constant-current source/limiter," 1997. [Online]. Available: https://www.vishay.com/docs/70596/70596.pdf

[9] [Online]. Available: http://kicad-pcb.org/about/kicad/

[10] Texas-Instruments, "Opa2211-ep low-power, precision operational amplifier," 2015. [Online]. Available: http://www.ti.com/lit/ds/sbos761/sbos761.pdf

[11] Fairchild-semiconductors, "Mmbf4391 / mmbf4392 / mmbf4393 n-channel switch," 1997. [Online]. Available: https://www.mouser.com/ds/2/149/PN4391-889992.pdf

[12] Fairchild-Semiconductors, "Mmbf4416 n-channel rf amplifiers," 2009. [Online]. Available: http://www.mouser.com/ds/2/149/MMBF4416-113958.pdf

[13] Central-semiconductors, "Cmldm8002a cmldm8002ag* cmldm8002aj surface mount silicon dual p-channel enhancement-mode mosfets," 2015. [Online]. Available: https://www.mouser.com/ds/2/68/cmldm8002a-369725.pdf

[14] R. A. Ryan *et al.*, "Design and operation of a cryogenic charge-integrating preamplifier for the MuSun experiment," *Journal of Instrumentation*, vol. 9, no. 07, pp. P07 029–P07 029, jul 2014. [Online]. Available: https://doi.org/10.1088%2F1748-0221%2F9%2F07%2Fp07029

[15] Analog-Devices, "High performance, 145 mhz fast fet op amps." [Online]. Available: https://www.analog.com/media/en/technical-documentation/data-sheets/AD8065_8066.pdf

[16] NXP-Semiconductors, "Bf862 n-channel junction fet," 2000. [Online]. Available: https://www.nxp.com/docs/en/data-sheet/BF862.pdf?

[17] MOXTEK, "N-channel ultra-low noise jfets." [Online]. Available: https://www.environmental-expert.com/files/50142/download/361832/3.pdf

[18] NXP-Semiconductors, "Bf998; bf998r silicon n-channel dual-gate mos-fets," 1996. [Online]. Available: https://www.nxp.com/docs/en/data-sheet/BF998.pdf?

6 Attachments

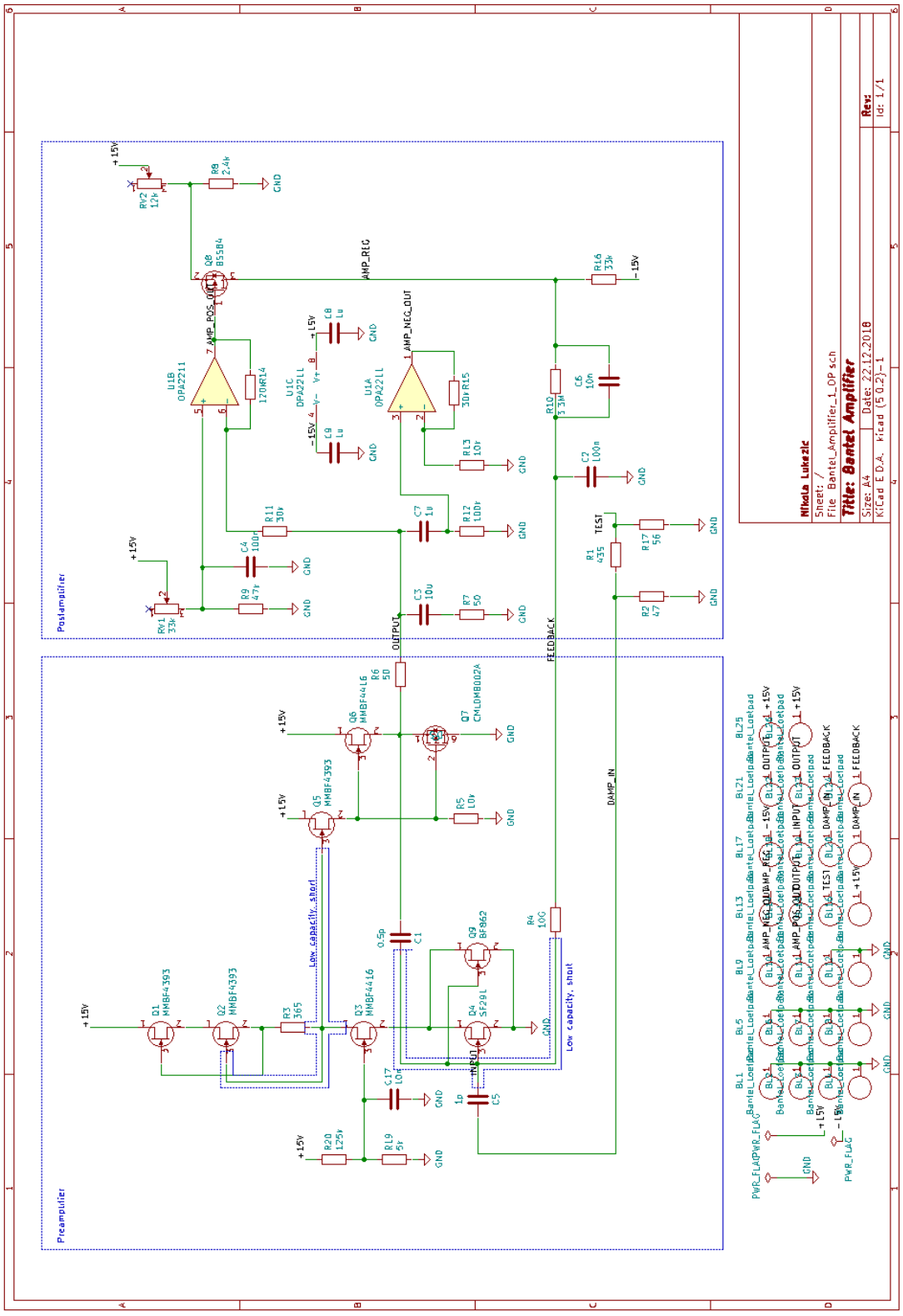

Figure 6.1: Full KiCAD schematic design

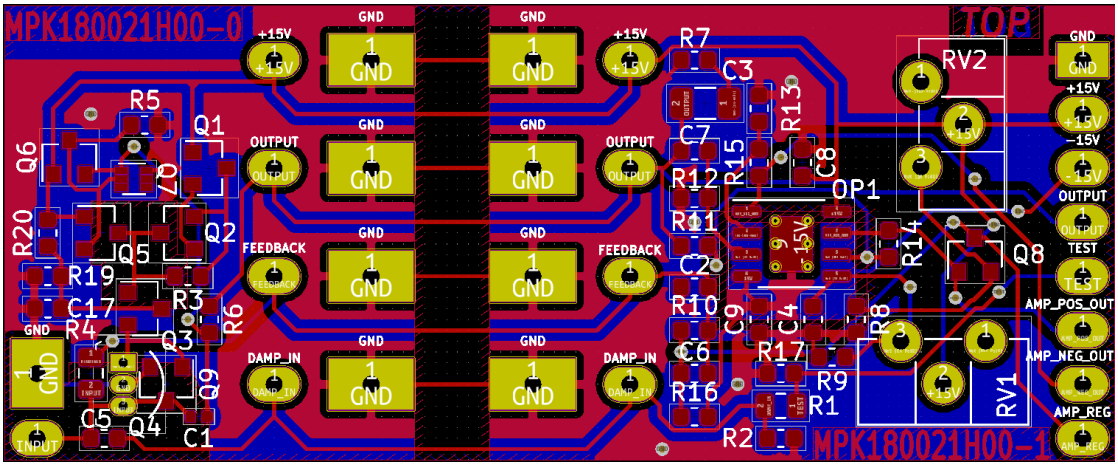

Figure 6.2: Top and bottom layers of the PCB design

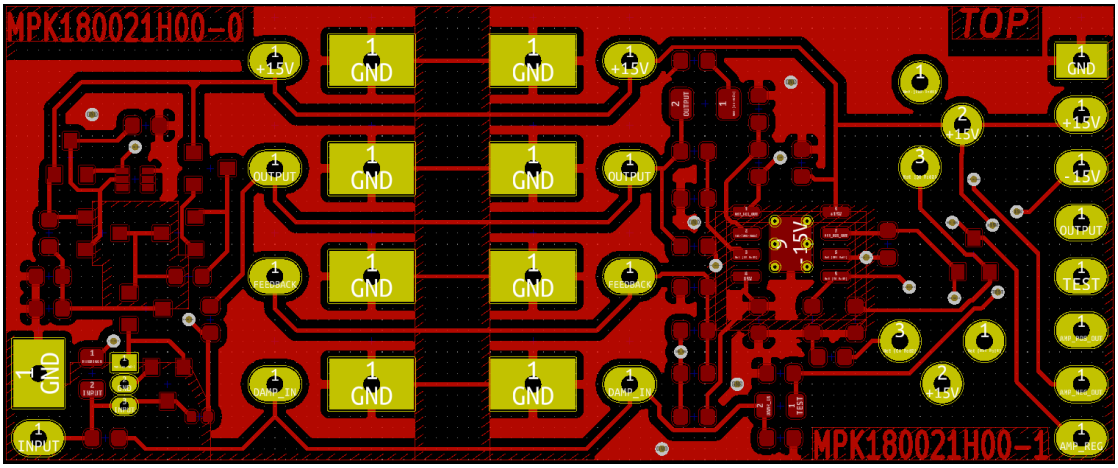

Figure 6.3: TOP layer of the PCB design

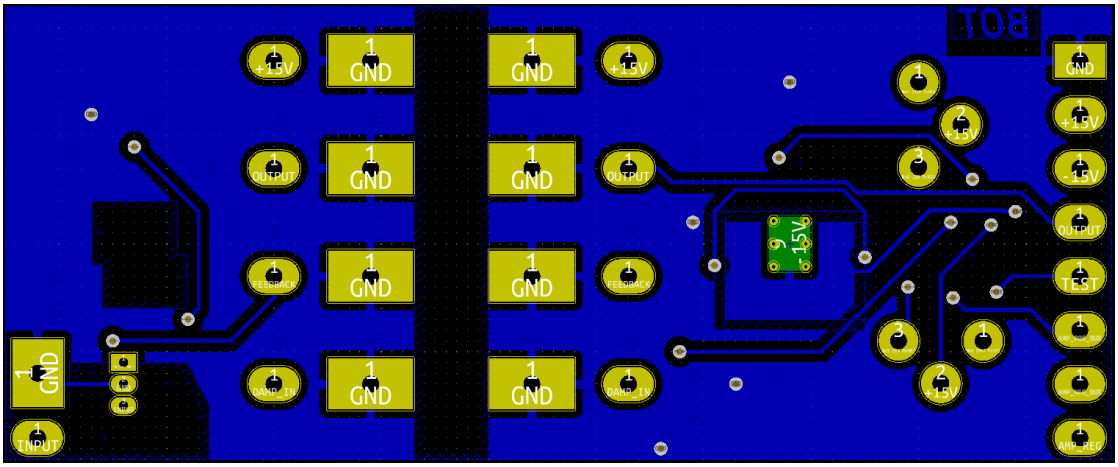

Figure 6.4: Bottom layer of the PCB design